

The Lyman-alpha Forest and Heavy Element Systems of GB1759+7539[★]

P. J. Outram¹, F. H. Chaffee², R. F. Carswell¹

¹ *Institute of Astronomy, Madingley Road, Cambridge CB3 0HA*

² *W. M. Keck Observatory, 65-1120 Mamalahoa Hwy., Kamuela, HI 96743, U.S.A.*

4 March 2019

ABSTRACT

We present observations of the high-redshift QSO GB1759+7539 ($z_{\text{em}} = 3.05$) obtained with HIRES on the Keck 10m telescope. The spectrum has a resolution of $\text{FWHM} = 7 \text{ km s}^{-1}$, and a typical signal-to-noise ratio per 2 km s^{-1} pixel of ~ 25 in the $\text{Ly}\alpha$ forest region, and ~ 60 longward of the $\text{Ly}\alpha$ emission.

The observed $\text{Ly}\alpha$ forest systems have a mean redshift of $\langle z \rangle = 2.7$. The H I column density distribution is well described by a power law distribution with index $\beta = 1.68 \pm 0.15$ in the range $13.5 < \log N < 14.5$. The Doppler width distribution is consistent with a Gaussian distribution of mean $b = 26 \text{ km s}^{-1}$, and standard deviation $\sigma = 12 \text{ km s}^{-1}$ with a cut-off at $b = 20 \text{ km s}^{-1}$. There is marginal evidence of clustering along the line of sight over the velocity range $100 < \Delta v < 250 \text{ km s}^{-1}$. The 1-point and 2-point joint probability distributions of the transmitted flux for the $\text{Ly}\alpha$ forest were calculated, and shown to be very insensitive to the heavy element contamination. We could find no evidence of Voigt profile departures due to infalling gas, as observed in the simulated forest spectra.

Twelve heavy-element absorption systems were identified, including damped Lyman-alpha (DLA) systems at $z_{\text{abs}} = 2.62$ and 2.91 . The C, N, O, Al, Si, P, S, Mg, Fe, and Ni absorption features of these systems were studied, and the elemental abundances calculated for the weak unsaturated lines. The systems have metallicities of $Z_{2.62} \simeq 1/20 Z_{\odot}$ and $Z_{2.91} \simeq 1/45 Z_{\odot}$. Both systems appear to have a low dust content. They show an over-abundance of α -elements relative to Fe-peak elements, and an under-abundance of odd atomic number elements relative to even. Nitrogen was observed in the $z_{\text{abs}} = 2.62$ system, and found to be under-abundant relative to oxygen, in line with the time delay model of primary nitrogen production. C II* was also seen, allowing us to determine an upper limit to the cosmic microwave background temperature at $z = 2.62$ of $T_{\text{CMB}} < 12.9 \text{ K}$.

Key words: cosmology: cosmic microwave background - galaxies: abundances - intergalactic medium - quasars: absorption lines - quasars: individual (GB1759+7539)

1 INTRODUCTION

In recent years rapid progress has been made in observational and theoretical studies of $\text{Ly}\alpha$ absorption lines in the spectra of high-redshift QSOs. Large telescopes have given us the opportunity of studying the lines in much greater detail than ever before, with large gains in both resolution and signal-to noise ratio (S/N) (e.g. Hu et al. 1995; Kirkman and Tytler 1997). At the same time, recent cosmological simula-

tions, taking into account a photoionizing ultra-violet background, have suggested that the $\text{Ly}\alpha$ clouds at high redshift develop naturally in a hierarchical structure-formation scenario (e.g. Cen et al. 1994; Miralda-Escudé et al. 1996). The detailed study of the $\text{Ly}\alpha$ forest, and comparison with the results of such simulations is perhaps one of the best tests of cosmic structure-formation theories, providing a constraint in the era $2 < z < 5$.

The heavy element systems observed in the line of sight to QSOs also provide a wealth of information about the formation of structure at high redshift. Understanding the chemical evolutionary history of galaxies is fundamental to the study of galaxy formation. The largest heavy element

[★] Based on observations obtained at the W. M. Keck Observatory, which is jointly operated by the University of California and the California Institute of Technology.

Table 1. Journal of Observations

Dates	Exposure time (s)	Central wavelength (Å)
6 July 1997	9000	5390
6 July 1997	6000	5415
13 July 1997	6000	5390
13 July 1997	9000	5415

systems, damped Lyman-alpha systems (DLAs), are believed to be the progenitors of present day galaxies (Wolfe 1995). They dominate the mass of neutral gas at redshift $z \simeq 3$, a mass comparable with that of the stars in present day spiral disks, suggesting that DLAs are the source of most of material available for star formation at high redshift (Lanzetta et al. 1995)

Prochaska & Wolfe (1997) studied the kinematics of DLAs, concluding that there is evidence for rotation, supporting the theory that they are the progenitors of modern day disk galaxies. This result was disputed by Haehnelt, Steinmetz & Rauch (1997). CDM models infer that DLAs are more like the progenitors of dwarf galaxies, or galactic halos, a model that is backed by studies of heavy element abundances (Pettini et al. 1994; Lu et al. 1996a) which have found an abundance pattern more akin to halo stars than disk stars in our Galaxy.

Pettini et al. (1994) systematically studied the Zn, and Cr abundances in DLAs, and concluded that they had low metallicity, typically $Z_{\text{DLA}} \simeq 1/10Z_{\odot}$ at $z \simeq 2$, and that they have a much lower dust-to-gas ratio than the local interstellar medium. Although it is still unclear which population of galaxies give rise to DLAs, it is apparent that the gas in DLAs is at an early stage in the chemical evolution of the object, and so abundance studies should give us an insight into the early stages of galaxy evolution.

In this paper, we present observations and analyses of the absorption spectrum of the QSO GB1759+7539 ($z_{\text{em}} = 3.05$). In §2 we describe the observations and data reduction methods. The analysis of the absorption lines, and identification of the heavy element lines is discussed in §3. Then, in §4, we present the main observational results concerning the Ly α forest, including the column density, and Doppler width distributions, and the clustering properties, as indicated by the two point correlation function. The elemental abundances in the two damped systems are discussed in §5, where the dust content, and nucleosynthesis histories of the two objects are considered. §6 investigates the cosmic microwave background temperature at $z = 2.62$. The main conclusions are summarized in §7.

2 OBSERVATIONS AND DATA REDUCTION

The radio source, GB1759+7539 was selected from the Green Bank 5-GHz survey (Condon et al. 1989), and identified by Hook et al. (1996) as a high-redshift $z_{\text{em}} = 3.05$ radio-loud QSO. Hook et al. noted that this object is optically very bright and hence it is ideal for high resolution spectroscopic study.

The data used in the present study were obtained in two nights (see Table 1) using the High Resolution Echelle Spectrometer (HIRES) on the 10m Keck telescope (Vogt 1992),

with the TeK 2048x2048 CCD. The FWHM of the instrument profile was found to be about 7 km s^{-1} . The HIRES setup is such that complete spectral coverage is only possible for $\lambda < 5100\text{\AA}$, so we used two partially overlapping setups to obtain complete coverage over the wavelength range 4116 - 6540 Å. This leads to fairly large variations in the S/N from region to region in the final spectrum.

Each image was bias and flat-field corrected using IRAF routines. The cosmic rays were flagged using a median filter and given zero weight in the individual frames. The sky-subtracted optical spectra were then optimally extracted, along with a one-sigma error estimate, calibrated to vacuum heliocentric wavelengths, and flux calibrated.

Even after flux calibration, there were some inexplicable low-order variations in the flux level of some of the images. The variations were echelle order dependent, and therefore clearly instrument related. These were removed by picking an apparently unaffected frame as a template, fitting low-order polynomials to the ratio of each frame to the template, and dividing out the variations. This procedure also scaled each spectrum to the same flux level. As the resulting spectrum was used solely for absorption line studies, where the ratio of the line intensity to that of the continuum is important, but the actual flux is not, this should have little effect on any of the analysis.

The echelle orders were then resampled to the same dispersion, and added together weighted according to their S/N. Finally, any bad pixels that escaped attention earlier were corrected and flagged to get zero weight in the line fitting routines. Atmospheric molecular oxygen absorption was removed from the region 6280 - 6310Å by dividing by a template generated from a standard star observed at similar airmass.

The continuum level redward of the Ly α emission line was estimated by fitting cubic splines to regions free from absorption lines, using the IRAF continuum fitting routine. The continuum for the Ly α forest region was fitted using the small regions deemed to be free of absorption, interpolating between these regions with a low-order polynomial fit. The region containing O VI and Ly β emission was fitted separately, in a similar manner, but with a higher order polynomial fit. The resulting continuum appears to fit the data well; however, in regions where the fitted continuum was possibly not accurate, it was allowed to vary in the line fitting routine VPFIT (see later.) These variations were never found to be more than about 2% of the original fitted continuum level.

3 DATA ANALYSIS

Voigt Profiles were fitted to the absorption lines, using the software package VPFIT (Webb 1987; Cooke 1994), in order to determine the redshifts, column densities and Doppler widths of ions with observed absorption lines.

The procedure uses a reduced χ^2 technique, which adjusts the parameters of an initial guess in order to minimize the χ^2 value. The spectrum was fitted in sections, using the smallest regions possible, bounded by where the spectrum reaches the continuum level. After an initial guess, further lines were automatically added until the addition of extra components failed to significantly reduce the normalised χ^2

further (as described in Rauch et al. 1992). This usually resulted in a normalised $\chi^2 \sim 1.1$. Occasionally, such a good fit was not quite possible, due to narrow non-Gaussian noise spikes in the spectrum; probably caused by CCD defects, or cosmic rays not fully removed in the data reduction process.

In some spectral regions where the reduced χ^2 was greater than ~ 1.1 the VPFIT program attempted to reduce it further by adding weak narrow features fitted to what are evidently noise spikes. A feature of the fits to these features is that the parameter error estimates are large, so they were easily identifiable. To avoid the possibility of overfitting in this way, such features were removed and the spectral region refitted.

The Voigt profile fitting procedure does not necessarily give unique results (as noted by Kirkman & Tytler 1997.) Often from a slight change in the initial guess, the routine settles on different sets of Voigt profiles which both fit the same absorption feature, and satisfy the criteria for a satisfactory fit. The intrinsic errors quoted in this paper are just the formal parameter fitting errors, assuming that the fitted solution in terms of Voigt profiles is correct. Different fits can often yield different solutions with differences much greater than this intrinsic error. This is particularly noticeable for saturated lines, where formal errors in column density can be less than 0.1 dex, but an extra line can alter the fitted column density by 2 dex or more due to the position of the feature on the curve of growth. Therefore, in general, the column density of saturated lines is ignored in this paper, or a very generous lower limit is used.

All fitted lines in the forest were initially assumed to be Ly α . The heavy element systems longward of the Ly α emission line were analysed and all but three absorption lines were positively identified. The Ly α forest was then searched for any new lines belonging to known heavy element systems, before it was finally searched for new heavy element systems. All lines that were not positively identified as a heavy element absorption line have been identified as Ly α for the purposes of this paper.

Atomic data, including oscillator strength, rest-frame vacuum wavelength and radiation damping constant are taken from Morton (1991), with revised values from Tripp, Lu, & Savage (1996). We have adopted recent oscillator strength determinations for Ni II (Fedchak & Lawler 1999; Zsargó & Federman 1998), and the weak Mg II transitions (Fitzpatrick 1997). Ni II $\lambda 1317$ remains uncertain, and so this line was not used as a constraint.

3.1 Heavy element absorption systems

A total of twelve heavy element absorption systems were identified, ranging from a single C IV doublet, to the complex absorption systems at $z_{\text{abs}} = 2.625$ and $z_{\text{abs}} = 2.911$. Apart from the interest in the heavy element systems themselves, the identification of heavy element lines is crucial to minimise the contamination of the sample of Ly α lines with misidentified heavy element lines in order to study the Ly α forest. Below is a brief summary of the heavy element absorption systems observed.

$z_{\text{abs}} = 0.000$ (3 components)

Galactic absorption of Na I $\lambda\lambda 5891, 5897$ was observed. Three components were fitted, with blueshifts of 16 - 46

km s $^{-1}$

$z_{\text{abs}} = 1.348$ (3 components)

Three components of Fe II, $\lambda\lambda 2344, 2374, 2382, 2586$, and 2600, at redshifts $z_{\text{abs}} = 1.3479, 1.3481$, & 1.3485, were observed longward of the Ly α emission line. Al III $\lambda\lambda 1854, 1862$, the only other potentially observable heavy element line within the range covered, lies in the Ly α forest and is obscured by other absorption lines.

$z_{\text{abs}} = 1.8848$

A single narrow-component C IV doublet $\lambda\lambda 1548, 1550$ was clearly detected at $z_{\text{abs}} = 1.8848$ in the Ly α forest. No other heavy element lines were detected in this system.

$z_{\text{abs}} = 1.935$ (complex)

There is a complex heavy element system at $z_{\text{abs}} = 1.935$, with C IV, Si II, Si IV, Al II, and Al III absorption detected. The C IV $\lambda\lambda 1548, 1550$ absorption feature requires six components and has components at velocities of -150 and $+180$ km s $^{-1}$ relative to the central ones. It lies in the Ly α forest, and is blended with Si II $\lambda 1253$ at $z_{\text{abs}} = 2.625$ and Si II $\lambda 1304$ at $z_{\text{abs}} = 2.484$ as well as Ly α forest lines, so some confusion is possible. Si IV $\lambda 1402$, but not $\lambda 1393$ lies within the wavelength range observed, and has a similar structure to that of the C IV absorption. Si II $\lambda 1526$, and Al II $\lambda 1670$ both lie in the Ly α forest as well, but Al III $\lambda\lambda 1854, 1862$ was observed redward of the Ly α emission line. Absorption from these three lower-ionization lines was detected only from the central component.

$z_{\text{abs}} = 2.4390$

A single C IV doublet $\lambda\lambda 1548, 1550$ was clearly detected at $z_{\text{abs}} = 2.4390$, longward of the Ly α emission line. This corresponds to a Ly α line which, if it is also single, has column density $\log N(\text{H I}) = 14.6$. No other heavy element lines were detected for this system.

$z_{\text{abs}} = 2.484$ (complex)

The $z_{\text{abs}} = 2.484$ system has a complicated absorption structure. The Ly α feature has four main components, two at around $z_{\text{abs}} = 2.484$, and outlying components at around ± 250 km s $^{-1}$, all of which are saturated. The central components have strong low-ionization absorption lines: Si II $\lambda\lambda 1190, 1193, 1260, 1304, 1526$, O I $\lambda 1302$, Al II $\lambda 1670$, C II $\lambda 1334$, and Fe II $\lambda 1608$ as well as the higher ionization ions Si III, Si IV, C IV, whereas the outer systems only show absorption in the latter ions. C IV $\lambda 1548$ is heavily blended with Si IV $\lambda 1402$ at $z_{\text{abs}} = 2.84$. Al II $\lambda 1670$, Si II $\lambda 1526$, and Fe II $\lambda 1608$ all lie in clear parts of the spectrum and so are well constrained; however, the other lines all lie in the forest where confusion and blending are more likely. C II $\lambda 1334$ and Si IV $\lambda\lambda 1393, 1402$ in particular are heavily blended with Ly α .

$z_{\text{abs}} = 2.625$ (complex)

The damped Ly α system has a column density of $\log N(\text{H I}) = 20.761 \pm 0.007$. Redward of the Ly α emission line, Si IV $\lambda\lambda 1393, 1402$, Si II $\lambda 1526$, C IV $\lambda\lambda 1548, 1550$, Fe II $\lambda\lambda 1608, 1611$, Al II $\lambda 1670$ and Ni II $\lambda\lambda 1751, 1741, 1709, 1454$, and 1370 were observed. The Al II $\lambda 1670$ feature was blended with C IV $\lambda 1548$ at $z_{\text{abs}} = 2.91$.

Table 2. Measurements of the unsaturated ion species for the $z_{\text{abs}}=2.62$ System

Ion	$\log N \pm \sigma$	notes	$[Z/H]$
H I	20.761 ± 0.007		
C II*	12.808 ± 0.063	in forest	$< -0.81^a$
C IV	14.626 ± 0.005		
NI	14.985 ± 0.025	in forest	-1.83 ± 0.03
N V	13.429 ± 0.035	heavily blended	
Mg II	15.721 ± 0.059	heavily blended	< -0.57
Si IV	14.189 ± 0.005		
P II	13.179 ± 0.068^b	in forest	-1.16 ± 0.07
S II	15.212 ± 0.014	in forest	-0.82 ± 0.02
Fe II	14.936 ± 0.009		-1.34 ± 0.01
Ni II	13.889 ± 0.007		-1.12 ± 0.01

^a Assuming $T_{\text{CMB}} \propto (1+z)$ ^b Adopted value; corrected for Ly α obscuration.

The high ionization lines, C IV $\lambda\lambda 1548, 1550$, and Si IV $\lambda\lambda 1393, 1402$ show a single sharp component at $z_{\text{abs}} = 2.6216$, also seen in C II $\lambda 1334$, 200 km s^{-1} blueward of the main system, which is fitted by seven Voigt profiles.

Upon searching the Ly α forest, further absorption lines; NI $\lambda = 1199.5, 1200.2$, and 1200.7 , NV $\lambda\lambda 1238, 1242$, Mg II $\lambda\lambda 1239, 1240$, S II $\lambda = 1250, 1253$, and 1259 , P II $\lambda 1152$, Si III $\lambda 1206$, O I $\lambda 1302$, and C II $\lambda 1334$ were detected. Si II $\lambda = 1190, 1193, 1260$, and 1304 were detected in the Ly α forest and fitted simultaneously with the other lines from the same ion species redward of the Ly α emission. Ni II $\lambda 1317$ was also seen, but not used simultaneously in the fit with the other Ni II lines due to uncertainty in its oscillator strength. The NI $\lambda = 1199.5, 1200.2$, and 1200.7 absorption features were very distinct and virtually free from Ly α blending. Mg II $\lambda\lambda 1239, 1240$, on the other hand, was blended with H I, and so the column density derived can only be taken as an upper limit.

The main component of P II ($z_{\text{abs}} = 2.6252$) was clearly detected, but any components at a slightly higher redshift are blanketed by a Ly α line. Assuming, however, that the P II feature has the same shape as the other low ionization lines, the other components would have a column density of half a dex less than the main component observed. Correcting for this obscuration leads to an increase in the abundance of Phosphorus by 0.24 dex. S II $\lambda 1253$, and 1259 are blended, but S II $\lambda 1250$ is not, allowing an accurate determination of the abundance of Sulphur. Many of the heavy element lines were saturated, but amongst the low ionization species, abundances of S II, Fe II, Ni II, NI, and P II were determined. Excited C II* $\lambda 1335$ was also marginally detected. The velocity profiles of many of the absorption features detected for this system can be seen in figure 1.

$$z_{\text{abs}} = 2.7871$$

A single C IV doublet $\lambda\lambda 1548, 1550$ was clearly detected at $z_{\text{abs}} = 2.7871$, longward of the Ly α emission line. This corresponds to a Ly α line with column density $\log N(\text{H I}) = 14.5$.

$$z_{\text{abs}} = 2.795 \text{ (2 components)}$$

Two CIV doublets $\lambda\lambda 1548, 1550$ were detected at $z_{\text{abs}} =$

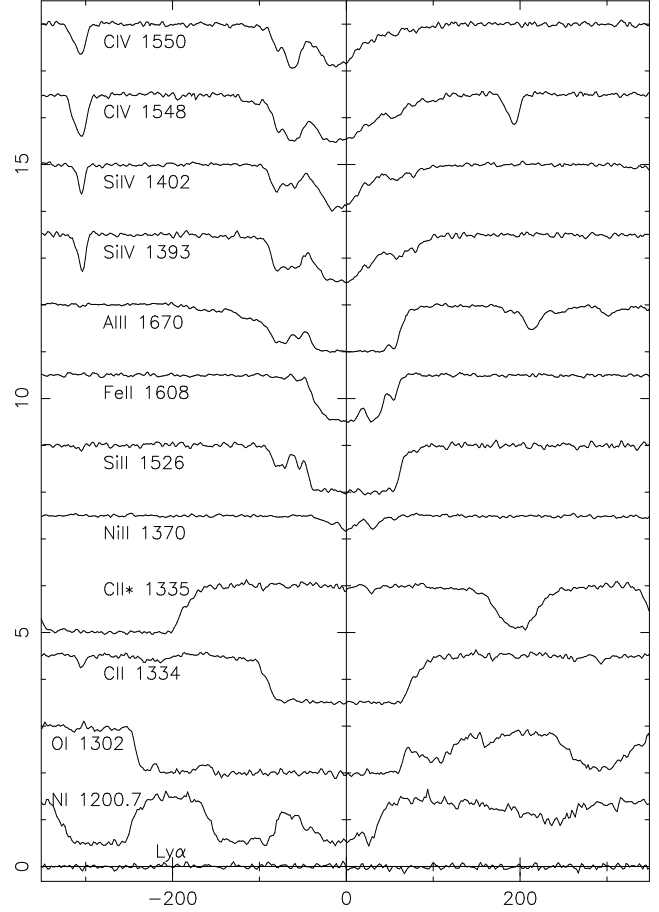


Figure 1. Velocity profiles (km s^{-1}) of heavy element lines in the $z_{\text{abs}} = 2.625$ DLA. The spectra are all normalized to unit continuum. The zero velocity is fixed at $z = 2.62528$. The O I line lies in the forest, and is blended with Si III from the $z = 2.91$ system. Blueward of the NI $\lambda 1200.7$ line, at $v = -250$ and -125 km s^{-1} can be seen the other two lines in the triplet; NI $\lambda\lambda 1199.5, 1200.2$.

2.795, & 2.796, corresponding to a Ly α line with column density $\log N(\text{H I}) = 16.2$.

$$z_{\text{abs}} = 2.835 \text{ (complex)}$$

C IV $\lambda\lambda 1548, 1550$ (five components) and Si IV $\lambda\lambda 1393, 1402$ (one component) were observed at $z_{\text{abs}} = 2.835$. The corresponding Ly α line has a column density of $\log N(\text{H I}) = 15.7$.

$$z_{\text{abs}} = 2.84 \text{ (complex)}$$

C IV $\lambda\lambda 1548, 1550$ absorption spanning a total velocity interval of 350 km s^{-1} , with 16 components, was observed at $z_{\text{abs}} = 2.84$. C II $\lambda 1334$, Si III $\lambda 1206$, and Si IV $\lambda\lambda 1393, 1402$ were also detected, showing a similar distribution. The saturated Ly α line has a measured column density of $\log N(\text{H I}) = 18.3$.

$$z_{\text{abs}} = 2.896 \text{ (3 components)}$$

Three C IV $\lambda\lambda 1548, 1550$ doublets were observed at $z_{\text{abs}} = 2.8954, 2.8956$, & 2.8973 , corresponding to two Ly α clouds of column density $\log N(\text{H I}) = 14.0$ & 14.2 .

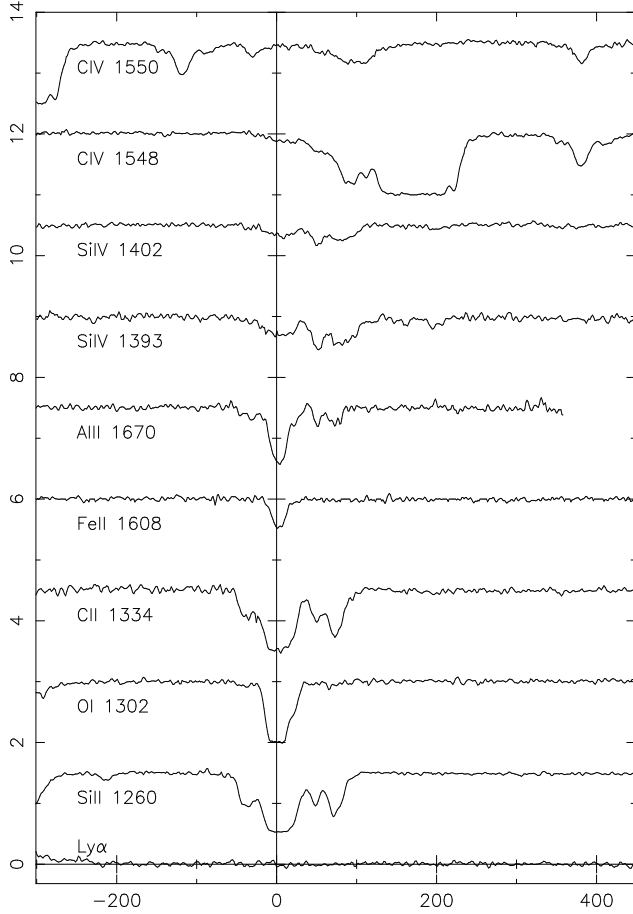


Figure 2. Velocity profiles (km s^{-1}) of heavy element lines in the $z_{\text{abs}} = 2.91$ system. The spectra are all normalized to unit continuum. The zero velocity is fixed at $z = 2.91016$. The saturated absorption feature partially obscuring C IV $\lambda 1548$ is Al II from the DLA system. The Al II feature for this system lies near the edge of the observed spectrum.

$z_{\text{abs}} = 2.910$ (complex)

The hydrogen column density of this large system is $\log N(\text{H I}) = 19.795 \pm 0.006$. There is a second Ly α component with $\log N(\text{H I}) = 17.021 \pm 0.205$ lying 420 km s^{-1} distant from the main system. Only C IV $\lambda\lambda 1548, 1550$ was detected for this component. C II $\lambda 1334$, C IV $\lambda\lambda 1548, 1550$, O I $\lambda 1302$, Al II $\lambda 1670$, Si II $\lambda = 1304$, and 1526 , Si IV $\lambda\lambda 1393, 1402$, and Fe II $\lambda 1608$ absorption features were all detected longwards of the Ly α emission line, and abundances were calculated for the unsaturated lines. Si II $\lambda = 1190, 1193$, and 1260 were detected in the forest and fitted, by seven components, simultaneously with the Si II lines redward of the Ly α emission. Both Si III $\lambda 1206$ and NV $\lambda\lambda 1238, 1242$ were tentatively seen in the Ly α forest, however the lines were very heavily blended in both cases. The velocity profiles of many of the absorption features identified from this system can be seen in figure 2.

A total of 721 lines were fitted, of which 324 are Ly α forest lines, 248 are heavy element lines redward of the Ly α emission (245 positively identified) and 149 are identified heavy element lines within the Ly α forest. The continuum-normalized spectrum, plotted against vacuum heliocentric

Table 3. Measurements for the $z_{\text{abs}} = 2.91$ System

Ion	$\log N \pm \sigma$	notes	$[Z/H]$
H I	19.795 ± 0.006		
C II	14.640 ± 0.023		-1.72 ± 0.02
C IV	13.852 ± 0.010		
N V	12.758 ± 0.116	heavily blended	
Al II	12.894 ± 0.008		-1.38 ± 0.01
Si II	14.166 ± 0.007		-1.18 ± 0.01
Si III	14.541 ± 0.262	heavily blended	
Si IV	13.479 ± 0.005		
Fe II	13.658 ± 0.010		-1.65 ± 0.01

wavelength(\AA), together with overlying profile fits, and the 1σ error are shown in figure 3. There are a number of spikes in the error due to cosmic rays or CCD defects. The error spikes around 6280\AA are due to molecular oxygen absorption that was removed from the spectrum. The tick marks indicate the positions of line features. A list of the line identifications, together with the fitted parameters is given in table 4.

4 THE LYMAN-ALPHA FOREST

With one line in three positively identified as a heavy element line within the Ly α forest region of the spectrum, the risk of contamination from further unidentified heavy element lines in the sample of H I lines appears large. Heavy element lines fitted as hydrogen tend to have very small Doppler parameters and large column density errors.

The Ly α lines were fitted without the additional constraint of higher-order lines, as the observed spectrum only covered a small fraction of the Lyman- β region. For some features, especially where Ly α clouds are blended with saturated heavy element features, the Voigt profile fit can be ill-constrained, and lead to H I column densities with large errors. We attempted to minimize contamination, and remove ill-constrained lines using an estimated error cutoff of $\sigma_{N(\text{H I})} = 0.5$ dex. Only two such H I lines appear, and both were simultaneously rejected using other criteria.

Incompleteness is a problem at the low column density end of the distribution. Line blending, where two or more lines cannot be individually resolved and hence are fitted by a single Voigt profile, is likely to give an over-density of broad lines and a paucity of low column density lines in the observed distribution relative to the intrinsic distribution. The probability of confusion due to cloud blending is high because of the large number of low density clouds. This is especially apparent for lines with $N(\text{H I}) < 10^{13} \text{ cm}^{-2}$. Some weak lines, especially broad ones, may also be missed simply due to the finite S/N, and uncertainty in the continuum level. In the fitting process, the maximum Doppler parameter allowed was 100 km s^{-1} , because very few lines larger than this are expected, and they would tend to be very poorly constrained, and could be artifacts of the fitted continuum level.

The effect of line blanketing, where weak lines are lost in the absorption profile of a stronger line, will also lead to an under-density of weak lines. The sample contains a few low-b lines with low column densities, $N(\text{H I}) < 10^{13} \text{ cm}^{-2}$, that

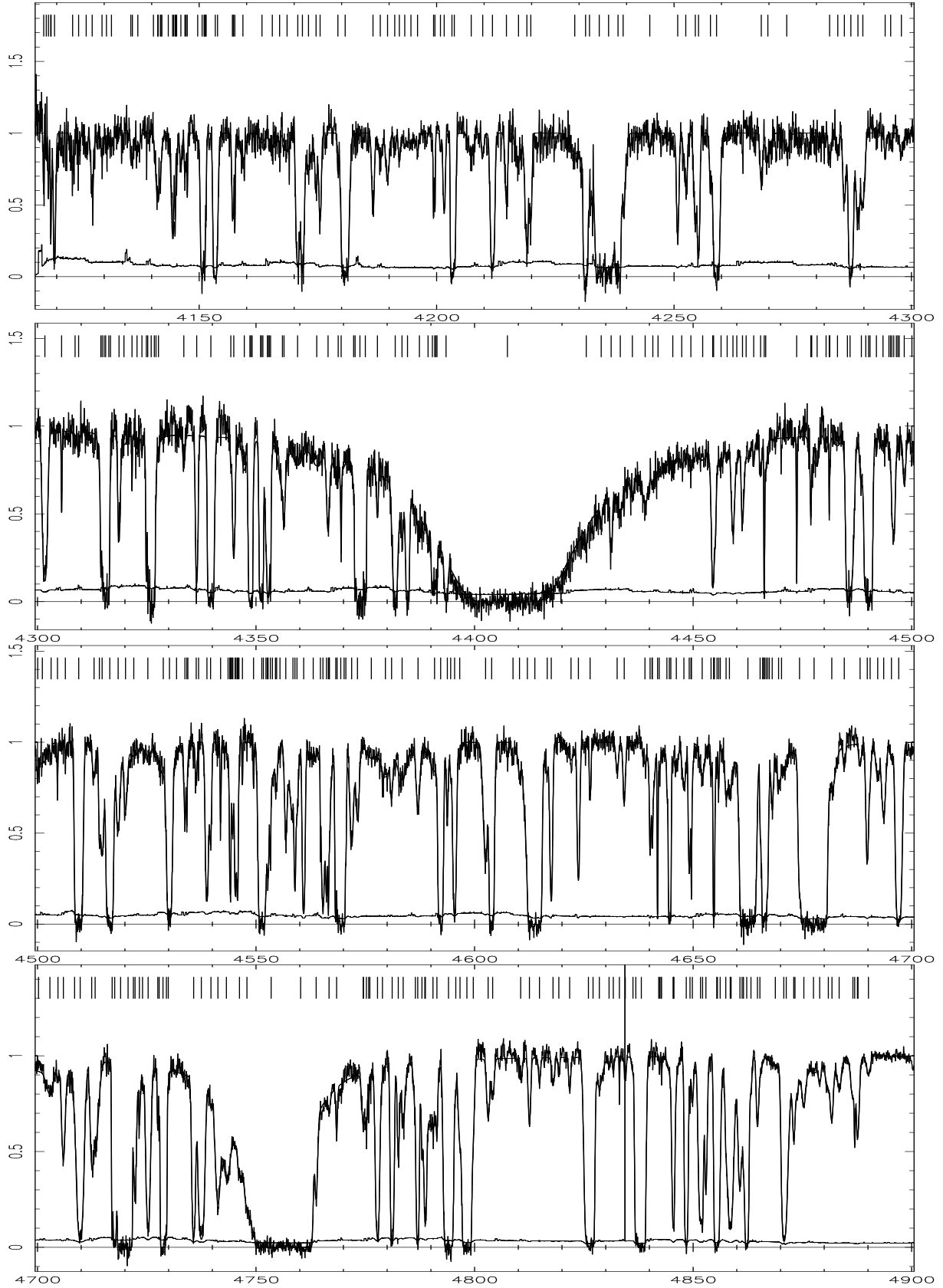


Figure 3. The spectrum of GB1759+7539, plotted against vacuum heliocentric wavelength(Å), normalized to unit continuum, together with overlying profile fits. The tick marks show the position of the components given in Table 4. The 1σ error is also shown.

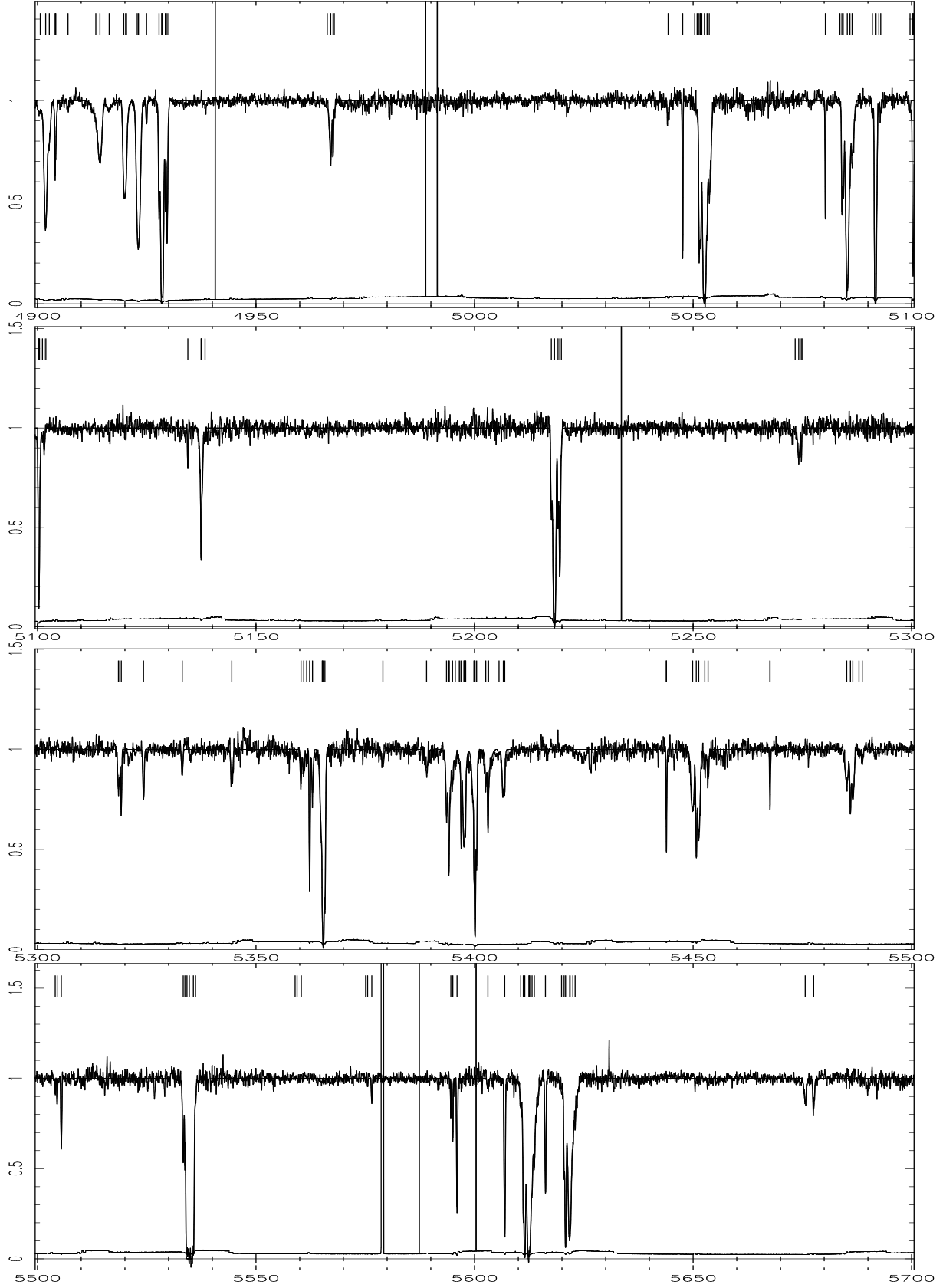


Figure 3. The spectrum of GB1759+7539, plotted against vacuum heliocentric wavelength(Å), normalized to unit continuum, together with overlying profile fits. The tick marks show the position of the components given in Table 4. The 1σ error is also shown.

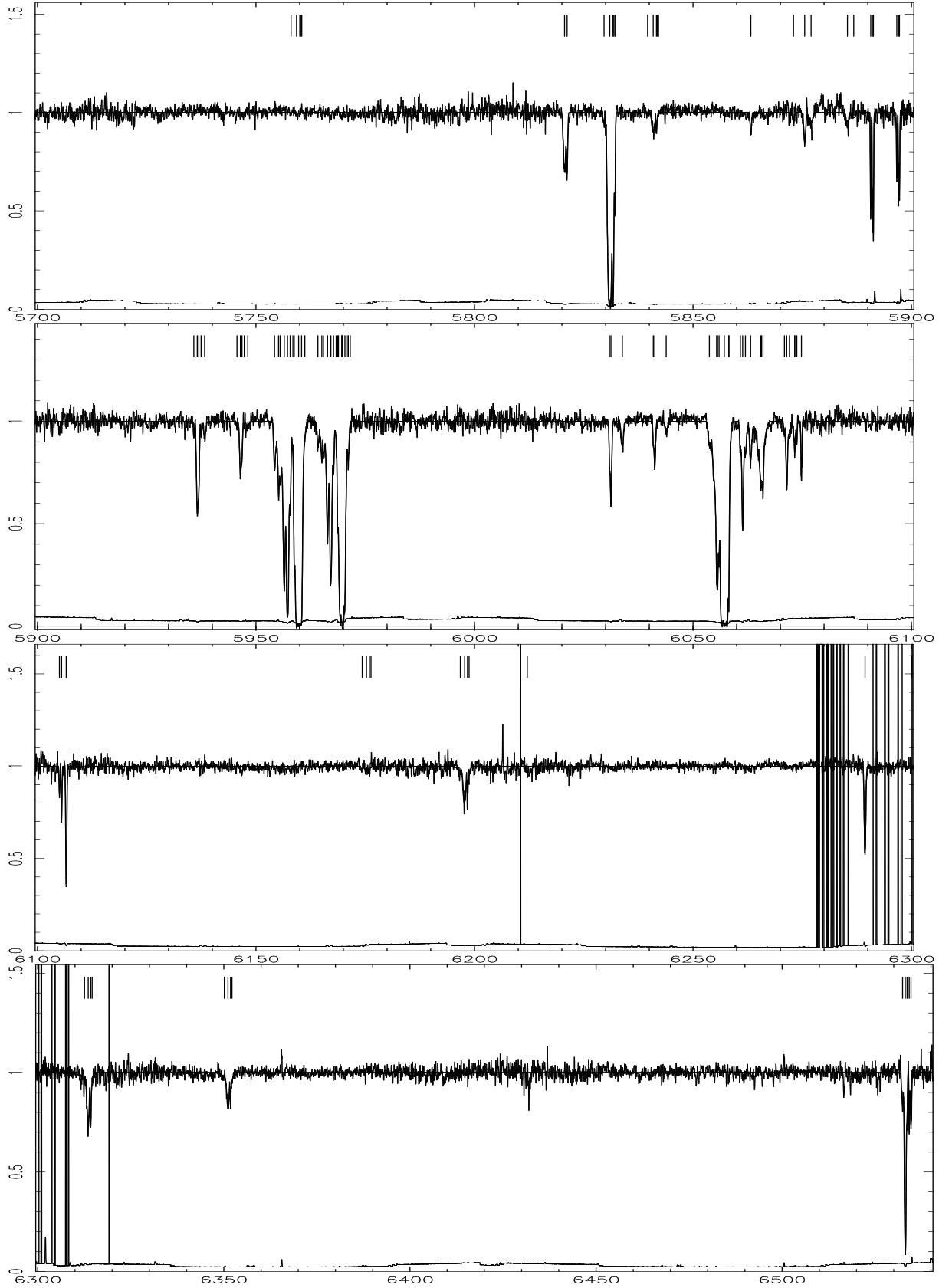


Figure 3. The spectrum of GB1759+7539, plotted against vacuum heliocentric wavelength(Å), normalized to unit continuum, together with overlying profile fits. The tick marks show the position of the components given in Table 4. The 1σ error is also shown.

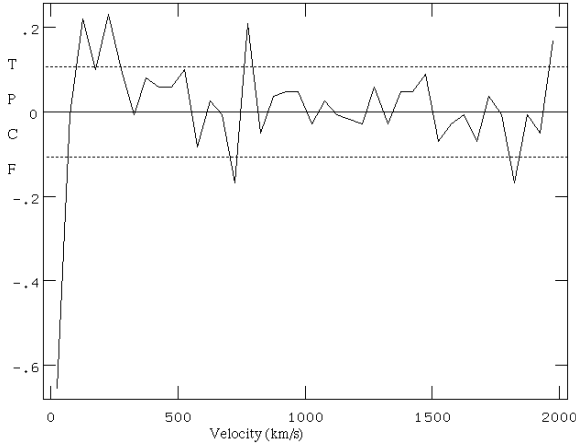


Figure 4. The two point correlation function vs. velocity separation for the entire sample of lines. The dashed lines show the 1σ errors.

are more likely to be fitted noise features than the intrinsic distribution (Rauch et al. 1992).

To avoid any adverse effects from the proximity effect, all Ly α clouds within 8 comoving Mpc of the QSO (38 in total) were left out. Only those lines with $13.5 < \log N < 14.5$, were used to obtain a complete sample with reliable column density determinations. Finally, an error cutoff of $\sigma_{N(\text{H I})} < 0.5$ dex, and $\sigma_b < \text{Max}[10, 10\sqrt{b/20}]$ was used, eliminating a further 2 systems, in order to minimise the effects outlined above. After all these restrictions were taken into account, our final sample consisted of 66 lines.

The column density and Doppler parameter distributions are in good agreement with those derived by Hu et al. (1995), Lu et al (1996b) and Kirkman & Tytler (1997). Over the limited range in column density available ($13.5 < \log N < 14.5$), the column density distribution is consistent with a single power-law with index $\beta = 1.68 \pm 0.15$. The Doppler parameter distribution peaks at around $b = 23 \text{ km s}^{-1}$, with a cut-off below about $b = 18 \text{ km s}^{-1}$, and a large tail towards high b -values. It is best fit by a Gaussian of mean $b = 26 \text{ km s}^{-1}$, and standard deviation $\sigma = 12 \text{ km s}^{-1}$ with a cut-off at $b = 20 \text{ km s}^{-1}$. No correlation was seen between the column density and Doppler width of the lines.

4.1 Clustering properties

To investigate the clustering properties of the forest lines we calculated the two point correlation function (TPCF)

$$\xi(v) = \frac{N_{\text{obs}}(v)}{N_{\text{exp}}(v)} - 1 \quad (1)$$

where $N_{\text{obs}}(v)$ is the number of observed pairs at separation v , and $N_{\text{exp}}(v)$ is the number of expected pairs if the lines were randomly distributed along the line of sight. $\xi(v)$ is shown in figure 4. The TPCF shows a deficit of 61 lines pairs with separations below 50 km s^{-1} . As the most likely b -value was found to be about 25 km s^{-1} , and a significant number of lines had Doppler widths considerably larger than this, the deficit could entirely be due to line blanketing, where one line obscures another, or line blending, where two lines would be fitted as one. These blended lines could also help ex-

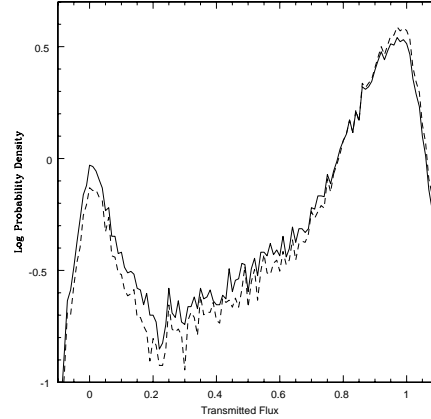


Figure 5. The flux distribution at $z \geq 2.7$. The solid line is the result for the whole Ly α forest spectrum, except for the damped systems which were removed. For the dashed line, all of the identified heavy element lines were removed as well.

plain the non-Gaussian tail in the b -distribution. This effect could also lower the observed value of $\xi(v)$ for $50 < \Delta v < 100 \text{ km s}^{-1}$, and so we shall focus on correlations on scales larger than this.

There is only marginal evidence of clustering along the line of sight over the velocity range $100 < \Delta v < 250 \text{ km s}^{-1}$. We find $\langle \xi \rangle = 0.18 \pm 0.06$ over this range. There is no evidence for any clustering on scales larger than this. This result is similar to that of Hu et al. (1995) who found 0.17 ± 0.045 over the range $50 < \Delta v < 150 \text{ km s}^{-1}$. Lu et al. (1996b) also noted a weak, statistically marginal, clustering signal over a similar velocity range. Cristiani et al. (1997) found a small but significant signal at $\Delta v = 100 \text{ km s}^{-1}$ of $\langle \xi \rangle = 0.2 \pm 0.04$. Further analysis showed that the signal was due to strong clustering in the larger Ly α clouds, and that lines with $N(\text{H I}) < 10^{13.6} \text{ cm}^{-2}$ showed no evidence for clustering. Crofts (1989), Chernomordik (1995), and Hu et al. (1995) have also noted a stronger correlation with larger clouds. Kirkman & Tytler (1997), however, found no signal on any scale, with $\langle \xi \rangle = 0.06 \pm 0.045$ in the range $50 < \Delta v < 150 \text{ km s}^{-1}$.

Cen et al. (1997) analysed Ly α clouds in simulated spectra, using a Λ CDM model, and predicted a significant positive correlation of $\langle \xi \rangle = 0.1 - 1.0$ on separations of $50 < \Delta v < 300 \text{ km s}^{-1}$ at $z=3$. Due to the finite box size, this is in fact an underestimate of the correlation in these simulations. Our results are in line with the lower end of the prediction, but rule out clustering on a scale $\langle \xi \rangle > \sim 1.0$.

4.2 The 1-point and 2-point joint probability distribution

The recent N-body cosmological simulations of the Ly α forest (e.g. Cen et al. 1994; Miralda-Escudé et al. 1996) have called into question the physical meaning behind the Voigt profile fitting procedure. In the past, Ly α clouds were viewed as discrete clouds confined by pressure or gravity within the intergalactic medium (IGM). If these clouds had a Gaussian velocity dispersion then the Voigt profile would describe the resulting line profile, and the physical column density

and Doppler width parameters could be estimated. The new paradigm, brought about by the cosmological simulations, views the Ly α forest as fluctuations in the IGM itself. Some of the Ly α forest lines in the simulations are seen to be non-Voigt, due to gravitational infall, or flows in the IGM. In the simulation models, the Ly α clouds have a variety of shapes and sizes, from nearly spherical clouds, to elongated filamentary structures, and cannot be described by a simple model (Cen and Simcoe 1997).

The Voigt profile analysis also has large intrinsic uncertainties due to line blending seen in high quality, high redshift data. Different initial guesses, and number of lines fitted to a region may determine different local minima in the χ^2 parameter space (Kirkman & Tytler 1997). This non-uniqueness is not helped by increasing S/N. This has led to the consideration of other statistics when comparing the observed quasar absorption spectra with those from simulations. Following Miralda-Escudé et al. (1997), we have measured the 1-point, and 2-point joint probability distribution of the transmitted flux in the Ly α forest spectrum of GB1759+7539.

The Ly α forest region of GB1759+7539 is very rich in heavy element features, with over 30% of the Voigt profiles fitted positively identified as heavy element lines. Heavy element absorption lines tend to be much narrower than Ly α lines, due to the lower thermal velocity dispersion of the heavier ions. We have investigated the effect that heavy element contamination has on the flux statistics, to test their discriminatory power.

The 1-point and 2-point joint probability distribution of the transmitted flux were calculated on the whole available spectrum, excluding the regions where the damping wings of the two large systems suppressed the spectrum. The results are shown as the solid lines in figures 5 and 6. Then, in order to investigate the effect of the heavy element features, all of the identified heavy element lines were masked off, and the distributions were calculated again. The results for the heavy element-free regions of the spectrum are shown as the dashed lines in figures 5 and 6.

It is clear, from studying figure 5, that the effect of masking out the heavy element lines is to slightly raise the average transmitted flux. This is to be expected, as only regions where heavy element absorption was present were masked off, and not regions where no absorption was seen. The shape of the flux probability distribution, however, appears almost unchanged.

The effect of raising the average transmitted flux when the heavy element lines are masked off also explains the higher levels of the mean flux difference at high velocity separations in the heavy element-free spectrum seen in figure 6. The shape of the 2-point joint probability distribution at separation velocities $\delta v < 100 \text{ km s}^{-1}$ is a good indication of the mean profile of the absorption lines. For $0.0 < F < 0.1$, the curve depends on the mean shape of saturated lines, whereas the $0.6 < F < 1.0$ curve is sensitive to weak absorbers. It can be seen, however, that there is virtually no difference between the two samples, with and without the heavy element lines. This indicates that the statistic does not detect heavy element contamination, or equivalently, it is not a good discriminator between samples where a large minority of lines are drawn from a different, intrinsically nar-

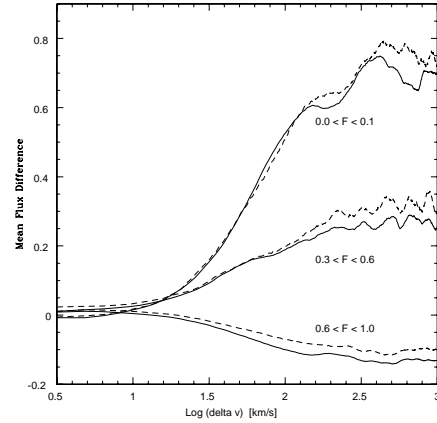


Figure 6. The mean flux difference distribution at $\langle z \rangle = 2.7$, averaged over the flux intervals F as indicated in the figure. The solid lines are the results for the whole Ly α forest spectrum, except for the damped systems which were removed. For the dashed lines, all of the identified heavy element lines were removed as well.

rower distribution, and samples where no such narrow lines are present.

4.3 Departures from the Voigt profile

A clear signature of deviations from Voigt profiles is observed in the simulated forest spectra (Miralda-Escudé et al. 1996), typically in systems still in a collapse phase. The cool, dense gas in its core produces a high column-density, narrow component, whereas the bulk motion, and shock-heating of the infalling material typically produces a broader component (Rauch 1996), producing departures, often asymmetric, from the Voigt profile. Although Voigt profile fitting yields an excellent fit to the data, it is expected that information about this intrinsic non-Voigtiness is contained in the way that small, or broad lines cluster about intermediate strength Ly α lines.

In order to investigate this, we decided to remove all of the strong Ly α lines from the spectrum, leaving just the small clouds that may show some such evidence of clustering. This was achieved by dividing the spectrum of GB1759+7539 by the Voigt profile fits of all heavy element lines, and all the hydrogen lines of Ly α forest clouds with a column density $N(\text{H I}) > 10^{13} \text{ cm}^{-2}$. All points of the spectrum with a flux level of less than 0.2 times the continuum level were not included in the division, and were then given zero weighting in the following addition. This spectrum should therefore still contain the signature of the small infalling clouds, which would tend to be fitted with Voigt profiles of column density $N(\text{H I}) < 10^{13} \text{ cm}^{-2}$, with the central narrow components now removed. Although this signature would be difficult to see in any single system, due to the low S/N and blending effects, it can be searched for statistically by stacking many such systems with the central Ly α component removed. If the departures from a Voigt profile were significant, one would expect to see a slight dip in the residual flux either side of the central wavelength in this composite spectrum.

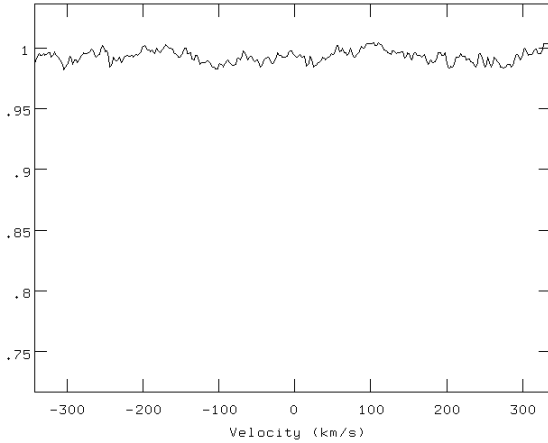


Figure 7. Composite spectrum for 150 H I lines with column densities in the range $10^{13} < N(\text{H I}) < 10^{14} \text{ cm}^{-2}$, after division by the Voigt profile fit, as described in the text. The spectrum is shown in velocity space relative to H I $\lambda 1215.67 \text{ \AA}$.

A composite spectrum was formed by shifting the divided spectrum of each system to the rest frame of the removed Ly α line, rebinning onto a common velocity scale, and averaging all such rest-frame spectra, using variance weighting. 150 intermediate strength ($10^{13} < N(\text{H I}) < 10^{14} \text{ cm}^{-2}$) Ly α lines were used, giving a final S/N ~ 400 . The composite spectrum can be seen in figure 7.

There is no evidence in the composite spectrum (figure 7) of Voigt profile departures due to infalling gas, as described in Miralda-Escudé et al. . The spectrum shows no significant dip either side of the central wavelength, and is consistent with the smaller Ly α lines being distributed randomly along the line-of-sight. Different column density limits, both for the summation, and for inclusion in the division were also used, but the results were similarly featureless. Similar tests need to be performed on simulated data to see if this constraint is an important one.

5 THE HEAVY ELEMENT SYSTEMS

In the line of sight to GB1759+7539 there are two large systems with conspicuous damping wings, as well as numerous smaller heavy element systems. One of the two systems has a column density $N(\text{H I}) > 2 \times 10^{20}$; the established, yet somewhat arbitrary criterion for a damped Lyman-alpha system (DLA) (Wolfe et al. 1986). The other system has a slightly lower column density ($N(\text{H I}) = 6 \times 10^{19}$), but displays similar properties to the larger DLAs. In this section we will study the elemental abundances of these two systems. We will only consider those abundance measurements that appear free from saturation effects, and use Fe as the metallicity indicator. The effects of dust on the measured abundances, the ratios of elements produced in different nucleosynthesis processes, and the implications for galactic chemical evolution will be discussed.

5.1 Dust depletion

In the diffuse inter-stellar medium (ISM) clouds, the relative intrinsic abundances are believed to be solar, and so any departures are thought to be due to varying levels of dust depletion (Savage and Sembach 1996). The refractory elements, with a high condensation temperature, are heavily depleted by the formation of dust grains, whereas the abundance of elements with a low condensation temperature is largely unaffected. Generally, the elements S, P, Zn, C, N, and O are depleted by a factor about 3 or less, but elements Si, Fe, Cr, Al, and Ni are much more heavily depleted in the ISM.

High redshift, young galaxies may have a different chemical enrichment pattern than present day galaxies, due to the different timescales of the various nucleosynthesis processes. In order to objectively study the dust depletion seen in DLAs, one therefore needs to compare the abundances of elements produced in the same nucleosynthesis processes that have very different depletion patterns. Vladilo (1998) studied the abundances of Zn, Fe, and Cr in a sample of 17 DLAs, and concluded that the dust-to-gas ratio was between 2 and 25 % of the Galactic value. This is in good agreement with the value of 5 - 20 % estimated by Pei, Fall & Bechtold (1991) from their study of the reddening of QSOs with foreground DLA absorption. Pettini et al. (1997a) concluded that the “typical” dust-to-gas ratio of DLAs is only $\sim 1/30$ of that of the Milky Way. Lu et al. (1996a), however, assert that there is no significant evidence for any dust depletion and that the overabundance of Zn relative to Cr may be intrinsic.

5.2 Nucleosynthesis and abundance ratios

Detailed abundance analysis of the disk and halo stars has provided evidence of the chemical evolution of our Galaxy (McWilliam 1997). The chemical composition of low mass stars has changed little since their formation, and so by studying the abundance ratios in old, low metallicity stars, we can learn about the nucleosynthesis processes that took place when our Galaxy was forming.

The halo stars have an average metallicity of $[\text{Fe}/\text{H}] \sim -1.6$. They have enhanced $[\alpha/\text{Fe}]$ ratios (where α includes O, Mg, Si, and S) by a factor of about 3 relative to solar (McWilliam 1997) due to the $\sim 10^8$ year time delay between α -element producing SNII and the first SNIa; the main source of Fe-peak elements (Tinsley 1979). This overabundance has also been observed in DLAs (Lu et al. 1996a; Pettini et al. 1995).

The production of odd atomic number elements depends on the neutron excess, which in turn depends on the initial metallicity of the nuclear fuel (Truran & Arnett 1971). This leads to an under-abundance of odd elements, relative to the even atomic number α -elements (e.g. $[\text{Al}/\text{Si}]$) at low metallicity. The $[\text{Al}/\text{Fe}]$ ratio, however, increases slightly with decreasing metallicity in Galactic stars (McWilliam 1997) indicating that Al could be classified as a mild α -element phenomenologically despite having an odd number of protons.

Some chemical evolution models also predict that nitrogen may be underabundant relative to oxygen in young high redshift objects, due delayed release of primary nitrogen in

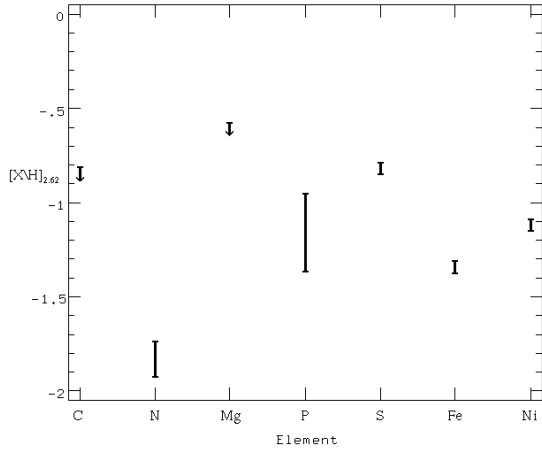


Figure 8. Observed elemental abundances relative to solar for the $z_{\text{abs}} = 2.625$ DLA plotted on a logarithmic scale. The errors, and limits are intrinsic and given to 3σ . The upper limit for C II is derived by considering the abundance of C II* and the temperature of the cosmic microwave background at that epoch.

intermediate mass stars relative to oxygen from high mass stars (Vila-Costas & Edmunds 1993). This effect, however, has not been convincingly seen in H II regions of nearby heavy element-poor galaxies (Thuan et al. 1995), or in blue compact galaxies (Izotov & Thuan 1999). It has been investigated in high redshift DLAs by Pettini et al. (1995) and Lipman et al. (1995). Later Lu et al. (1998) found a large scatter in the N/Si ratio, so giving support for the time-delay model of primary N production.

5.3 The Damped Ly α System at $z_{\text{abs}} = 2.625$

The measured abundances for the $z_{\text{abs}} = 2.625$ DLA are listed in table 2, and plotted in figure 8. The velocity profiles of many of the absorption features can be seen in figure 1. In calculating the abundances, it was assumed that the ion species observed were from the dominant ionization stages in HI gas, so that corrections for other ionization stages are negligible. Given the large HI column density of the system, this is believed to be a good assumption (Viegas 1995). Also, it is assumed that the HI column density is a good measure of the hydrogen content of the system, since the fraction of molecular hydrogen is known to be small (Levshakov et al. 1992).

Another source of uncertainty is that, as seen in the velocity profile of the heavy element lines, there are several components contributing to this system. In the H I feature, however, this structure is not seen, and it is possible that there may be a metallicity gradient, or additional components contributing to the Ly α line, but not the heavy element lines. We summed the column densities for the heavy element lines over all the components, and so are examining the average properties of the DLA. Although the metallicity may vary through the object, it appears, by comparing the column density of individual heavy element line components, that the relative abundances are fairly constant. The solar abundance values used in the calculation were taken from Anders & Grevesse (1989).

From the abundance of iron, $[\text{Fe}/\text{H}] = -1.34 \pm 0.01$, cal-

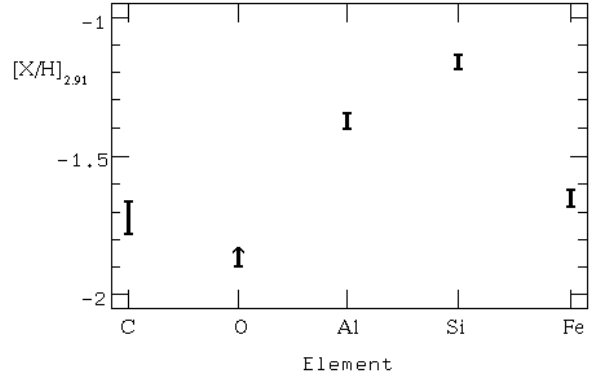


Figure 9. Observed elemental abundances relative to solar for the $z_{\text{abs}} = 2.911$ plotted on a logarithmic scale. The errors, and limits are 3σ .

culated using the unsaturated $\lambda = 1611$ line, we observe that the $z_{\text{abs}} = 2.625$ DLA has a metallicity $Z_{2.62} \simeq 1/20Z_{\odot}$, which is about typical for a DLA at this redshift (Pettini et al. 1997b). Hence, this galaxy is still in the early stages of its chemical evolution. Note, however, that in reaching this conclusion, it is assumed that there is little depletion of Fe onto dust grains. If much dust is present, the system would have a higher metallicity than estimated.

5.4 The System at $z_{\text{abs}} = 2.91$

The heavy element system at $z_{\text{abs}} = 2.91$ has a hydrogen column density of $\text{Log } N(\text{H I}) = 19.8$. The heavy element abundances were calculated as described above, assuming no ionization correction. Due to the smaller size, and lower metallicity of this system, different ion species were on the linear regime of the curve of growth, and hence the calculated abundances are for different species than the $z_{\text{abs}} = 2.625$ system. The measured abundances are listed in table 3, and plotted in figure 9. Assuming little dust depletion, the metallicity of this system is $Z_{2.91} \simeq 1/45Z_{\odot}$. The velocity profiles of many of the absorption features can be seen in figure 2.

5.4.1 Deuterium Abundance Determination?

Burles & Tytler (1998) attempted to determine the cosmologically important D/H ratio by observing the Ly α , Ly β , and Ly γ absorption line profiles of this system. They claim to have measured a value of $\text{Log}(\text{D}/\text{H}) = -4.3 \pm 0.3$. On the basis of the evidence presented here it is hard to see how this measurement could be reliable. Due to the high column density ($\text{Log } N(\text{H I}) = 19.8$) of the system, the hydrogen Ly α line (see figure 2), and to some extent the Ly β line, obscure the deuterium counterpart at -80 km s^{-1} . Several more Lyman series lines would be required to determine the intrinsic structure in the hydrogen absorption of the system, and distinguish this from any deuterium absorption, and any intervening Ly α features. The structure seen in the heavy element absorption lines of the system (7 components of Si II were fitted, spanning over 150 km s^{-1} ; see figure 2) suggests that even then an accurate determination may not be possible. Unfortunately, they published only the result, and not the full analysis.

5.5 Discussion: Dust and the intrinsic abundances

The over-abundance of sulphur relative to iron in the $z_{\text{abs}} = 2.62$ system, $[\text{S}/\text{Fe}]_{2.62} = 0.5$, and silicon in the $z_{\text{abs}} = 2.914$ system, $[\text{Si}/\text{Fe}]_{2.91} = 0.5$ is consistent with that seen in α -elements at this metallicity (McWilliam 1997). Since S is undepleted, yet Fe is heavily depleted by dust, the measurement for the $z_{\text{abs}} = 2.62$ system is consistent with a low level of dust depletion in the DLAs, with Fe depleted by no more than about 0.2 dex.

Chemical evolution models predict that there should be a large scatter in the values of $[\text{N}/\text{O}]$ due to the delayed release of primary nitrogen. In the $z_{\text{abs}} = 2.62$ DLA, the O I $\lambda 1302$ line is saturated, so a comparison with S is considered instead. This is based on the assumption that the ratio O/S is essentially solar. We find that $[\text{N}/\text{S}]_{2.62} = -1.0$, which is lower than that of the heavy element-poor H II regions, and consistent with the time-delay model of primary nitrogen production.

The abundance of phosphorus was measured at $[\text{P}/\text{Fe}]_{2.62} = 0.2$. In the smaller system, aluminium was observed, with $[\text{Al}/\text{Fe}]_{2.91} = 0.3$. P and Al have an odd number of protons, and so should be under-abundant relative to even atomic number elements. Indeed, $[\text{P}/\text{S}]_{2.62} = -0.3$, and $[\text{Al}/\text{Si}]_{2.91} = -0.2$ as expected. McWilliam (1997) noted that Na, and Al are have a slight over-abundance relative to Fe at low metallicities. Since P is formed from Al by the addition of an alpha-particle, it too should exhibit the same property. Our measured abundance is consistent with this.

The relative abundance of carbon, $[\text{C}/\text{Fe}]_{2.91} = -0.1$, in the smaller system has an essentially solar value. Wheeler et al. (1989) concluded that the abundance of carbon is essentially solar, irrespective of metallicity. A slight enhancement of C was observed in the Galactic disk at low metallicity (Tomkin et al. 1995), but this was not seen in halo stars (McWilliam et al. 1995). The important point is that carbon has not been seen to be *under*-abundant at any metallicity. Since carbon is relatively undepleted by dust, but iron is, any dust depletion in this system would lead to an intrinsic under-abundance of carbon, and so we conclude that the level of dust in the $z_{\text{abs}} = 2.91$ system must be very low.

Unfortunately, the abundances of two elements produced in the same nucleosynthesis processes, but with differing depletion patterns have not been observed. Hence, a direct estimate on the dust depletion is not possible. The abundance patterns observed in the two systems, however, are consistent with a low level of dust and the nucleosynthesis arguments considered above.

6 THE CMB TEMPERATURE AT $Z = 2.62$

According to Big Bang theory, the temperature of the cosmic microwave background (CMB) should increase linearly with $(1+z)$. The local background temperature has been accurately measured at 2.73K. Bahcall & Wolf (1968) suggested that by observing the relative populations of ground-state fine-structure lines of certain atoms, as seen in QSO absorption systems, one could estimate the temperature of the CMB at high redshift. In the last few years, several measurements at high redshift have been made, using the fine-structure levels of C I and C II (Songaila et al. 1994(a);

Songaila et al. 1994(b); Lu et al. 1996a; Lu et al. 1996c), all of which were consistent with the Big Bang prediction.

The C II line of the $z_{\text{abs}} = 2.62$ DLA was saturated. Therefore, in order to estimate an upper limit for the temperature of the CMB, we assume that $[\text{C}/\text{Fe}]_{2.62} > -0.3$ and hence that $\log N(\text{CII}) > 15.7$. The ratio $[\text{C}/\text{Fe}]$ is believed to be essentially solar at all metallicities (Wheeler et al. 1989), and the effect of any dust would be to increase the intrinsic metallicity, and hence the abundance of C. Therefore, we believe this to be a fair assumption. The velocity profile for the marginally detected CII* absorption feature can be seen in figure 1. Although the profile appears to match that of other low ionization lines (e.g. NiII) giving confidence in the identification, it lies in the Ly α forest, and hence there is the possibility of Ly α contamination. Therefore, we take an upper limit (3σ) of $\log N(\text{CII}^*) < 13.0$. The CII*/CII ratio then yields an upper limit of $T_{\text{CMB}} < 12.9\text{K}$ at $z = 2.62$. This is very close to the Big Bang cosmology prediction, $T_{\text{CMB}} = 9.9\text{K}$, at this redshift, which suggests that there is negligible excitation of the C II ions by other mechanisms.

7 SUMMARY AND CONCLUSIONS

We obtained an echelle spectrum of the high-redshift QSO GB1759+7539 ($z_{\text{em}} = 3.05$) using the instrument HIRES on the Keck 10m telescope. The spectrum has wavelength coverage 4100 - 6540Å, a resolution of FWHM=7 km s⁻¹, and a typical S/N per 2 km s⁻¹ pixel of ~ 25 in the Ly α forest region, and ~ 60 longward of the Ly α emission. Voigt profiles were fitted to all of the absorption features, and the heavy element lines from twelve heavy element systems were identified. The Ly α forest lines, and the absorption features of the two large systems were analysed in detail.

The observed Ly α forest systems have a mean redshift of $\langle z \rangle = 2.7$. The H I column density distribution is well described by a power law distribution with index $\beta = 1.68 \pm 0.15$ in the range $13.5 < \log N < 14.5$. The Doppler width distribution is consistent with a Gaussian distribution of mean $b = 26 \text{ km s}^{-1}$, and standard deviation $\sigma = 12 \text{ km s}^{-1}$ with a cut-off at $b = 20 \text{ km s}^{-1}$. There is marginal evidence of clustering along the line of sight over the velocity range $100 < \Delta v < 250 \text{ km s}^{-1}$. The 1-point and 2-point joint probability distributions of the transmitted flux in the Ly α forest region of the spectrum were calculated, and shown to be very insensitive to the heavy element contamination. We could find no evidence of Voigt profile departures due to infalling gas, as observed in the simulated forest spectra (Miralda-Escudé et al. 1996).

The C, N, O, Al, Si, P, S, Mg, Fe, and Ni absorption features of the large systems were studied, and the elemental abundances calculated for the weak unsaturated lines. The systems have metallicities of $Z_{2.62} \simeq 1/20Z_{\odot}$ and $Z_{2.91} \simeq 1/45Z_{\odot}$. Both systems appear to have a low dust content. They show an over-abundance of α -elements relative to Fe-peak elements, and an under-abundance of odd atomic number elements relative to even. N was observed in the $z_{\text{abs}} = 2.62$ system, and found to be under-abundant relative to O, in line with the time delay model of primary N production.

ACKNOWLEDGEMENTS

We would like to thank Sandra Savaglio, and an anonymous referee, for helpful comments. PJO acknowledges support from PPARC. Much of the data reduction and analysis was performed on the Starlink-supported computer network at the Institute of Astronomy.

REFERENCES

- Anders, E., Grevesse, N. 1989, *Geochim. cosmochim. Acta*, 53, 197.
- Bahcall, J.N., Wolf, R.A. 1968, *ApJ*, 152, 701.
- Burles, S., Tytler, D. 1998, *Space Sci. Rev.*, 84, 65.
- Cen, R., Miralda-Escudé, J., Ostriker, J.P., Rauch, M. 1994, *ApJ*, 437, 9.
- Cen, R., Phelps, S., Miralda-Escudé, J., Ostriker, J.P. 1998, *ApJ*, 496, 577.
- Cen, R., Simcoe, R.A. 1997, *ApJ*, 483, 8.
- Chernomordik, V.V. 1995, *ApJ*, 440, 431.
- Condon, J.J., Broderick J.J., Seielstad, G.A. 1989, *AJ*, 97, 1064.
- Cooke, A.J. 1994, Ph.D. thesis, Cambridge University.
- Cristiani, S., D'Odorico, S., D'Odorico, V., Fontana, A., Giallongo, E., Moscardini, L., Savaglio, S. 1997, in *Structure and Evolution of the IGM from QSO Absorption Line Systems*, eds. P. Petitjean, S. Charlot (Editions Frontières), 165.
- Crotts, A.P.S. 1989, *ApJ*, 336, 550.
- Fedchak, J.A., Lawler, J.E. 1999, *ApJ*, submitted.
- Fitzpatrick, E.L. 1997, *ApJ*, 482, L99.
- Haehnelt, M.G., Steinmetz, M., Rauch, M. 1998, *ApJ*, 495, 647.
- Hook, I.M., McMahon, R.G., Irwin, M.J., Hazard, C. 1996, *MNRAS*, 282, 1274.
- Hu, E.M., Kim, T-S., Cowie, L.L., Songaila, A. 1995, *AJ*, 110, 1526.
- Izotov, Y. I., Thuan, T. X. 1999, to appear in *ApJ*.
- Kirkman, D., Tytler, D. 1997, *ApJ*, 484, 672.
- Lanzetta, K.M., Wolfe, A.M., Turnshek, D.A. 1995, *ApJS*, 440, 435.
- Levshakov, S.A., Chaffee, F.H., Foltz, C.B., Black, J.H. 1992, *A&A*, 262, 385.
- Lipman, K., Pettini, M., Hunstead, R.W. 1995, in *QSO Absorption Lines*, ed. G. Meylan (Springer-Verlag), 89.
- Lu, L., Sargent, W.L.W., Barlow, T.A., Churchill, C.W., Vogt, S.S. 1996, *ApJS*, 107, 475 (a).
- Lu, L., Sargent, W.L.W., Womble, D.S., Takada-Hidai, M. 1996, *ApJ*, 472, 509 (b).
- Lu, L., Sargent, W.L.W., Womble, D.S., Barlow, T.A. 1996, *ApJ*, 457, L1 (c).
- Lu, L., Sargent, W.L.W., Barlow, T.A. 1998, *AJ*, 115, 55.
- McWilliam, A., Preston, G.W., Sneden, C., Shectman, S. 1995, *AJ*, 109, 2736.
- McWilliam, A. 1997, *ARA&A*, 35, 503.
- Miralda-Escudé, J., Cen, R., Ostriker, J.P., Rauch, M. 1996, *ApJ*, 471, 582.
- Miralda-Escudé, J., Rauch, M., Sargent, W. L. W., Barlow, T. A., Weinberg, D. H., Hernquist, L., Katz, N., Cen, R., Ostriker J. P. 1997, in *Structure and Evolution of the Intergalactic Medium from QSO Absorption Line Systems*, ed. P. Petitjean & S. Charlot (Editions Frontières), 155.
- Morton, D.C. 1991, *ApJS*, 77, 119.
- Pei, Y.C., Fall, S.M., Bechtold, J. 1991, *ApJ*, 378, 6.
- Petitjean, P., Webb, J.K., Rauch, M., Carswell, R.F., Lanzetta, K. 1993, *MNRAS*, 262, 499.
- Pettini, M., Smith, L.J., Hunstead, R.W., King, D.L. 1994, *ApJ*, 426, 79.
- Pettini, M., Lipman, K., Hunstead, R.W. 1995, *ApJ*, 451, 100.
- Pettini, M., King, D.L., Smith, L.J., Hunstead, R.W. 1997, *ApJ*, 478, 536 (a).
- Pettini, M., Smith, L.J., King, D.L., Hunstead, R.W. 1997, *ApJ*, 486, 665 (b).
- Prochaska, J.X., Wolfe, A.M. 1997, *ApJ*, 487, 73.
- Rauch, M., Carswell, R.F., Chaffee, F.H., Foltz, C.B., Webb, J.K., Weymann, R.J., Bechtold, J., Green, R.F. 1992, *ApJ*, 390, 387.
- Rauch, M. 1996, in *Cold Gas at High Redshift*, ed. Bremer, M.N. (Kluwer Academic Publishers).
- Savage, B.D., Sembach, K.R. 1996, *ARA&A*, 34, 279.
- Songaila, A., Cowie, L.L., Hogan, C., Rugers, M., 1994, *Nature*, 368, 599 (a).
- Songaila, A., Cowie, L.L., Vogt, S., Keane, M., Wolfe, A.M., Hu, E.M., Oren, A.L., Tytler, D. R., Lanzetta, K.M. 1994, *Nature*, 371, 43 (b).
- Thuan, T.X., Izotov, Y.I., Lipovetsky, V.A. 1995, *ApJ*, 445, 108.
- Tinsley, B.M. 1979, *ApJ*, 229, 1046.
- Tomkin, J., Woolf, V.M., Lambert, D.L. 1995, *AJ*, 109, 2204.
- Tripp, T.M., Lu, L., Savage, B.D. 1996, *ApJS*, 102, 239.
- Truran, J.W., Arnett, W.D. 1971, *Astrophys. Space Sci.*, 11, 430.
- Viegas, S.M. 1995, *MNRAS*, 276, 268.
- Vila-Costas, M.B., Edmunds, M.G. 1993, *MNRAS*, 265, 199.
- Vladilo, G. 1998, *ApJ*, 493, 583.
- Vogt, S.S. 1992, in *High Resolution Spectroscopy with the VLT*, ed. M-H Ulrich (Garching: ESO), 223.
- Webb, J.K. 1987, Ph.D. thesis, Cambridge University.
- Wheeler, J.C., Sneden, C., Truran, J.W. 1989, *ARA&A*, 27, 279.
- Wolfe, A.M. 1995, in *QSO Absorption Lines*, ed. G.Meylan (Springer-Verlag), 13.
- Wolfe, A.M., Turnshek, D.A., Smith, H.A., Cohen, R.D. 1986, *ApJSS*, 61, 249.
- Zhang, Y., Anninos, P., Norman, M.L. 1995, *ApJ*, 453, L57.

Table 4. Absorption line parameter list

ID	λ_{rest}	λ_{obs}	z	σ_z	b	σ_b	$\text{Log}N$	$\sigma_{\text{Log}N}$
Si IV	1402.77	4117.27	1.935102	0.000000	8.48	0.00	12.987	0.044
Si IV	1402.77	4117.80	1.935480	0.000000	7.93	0.00	12.407	0.150
Si IV	1402.77	4118.26	1.935805	0.000000	8.76	0.00	13.034	0.056
Si IV	1402.77	4118.72	1.936137	0.000000	5.27	0.00	12.995	0.214
H I	1215.67	4118.82	2.388111	0.000030	12.35	2.08	13.065	0.117
H I	1215.67	4119.53	2.388697	0.000010	19.36	1.28	13.730	0.035
H I	1215.67	4123.34	2.391830	0.000048	33.36	6.13	13.134	0.068
H I	1215.67	4124.61	2.392876	0.000070	25.84	9.12	12.779	0.127
H I	1215.67	4126.21	2.394188	0.000081	28.26	10.08	12.735	0.132
H I	1215.67	4127.48	2.395231	0.000020	25.76	2.41	13.308	0.036
H I	1215.67	4129.54	2.396926	0.000048	21.60	6.10	12.734	0.102
H I	1215.67	4130.46	2.397687	0.000058	17.51	7.73	12.523	0.159
H I	1215.67	4131.52	2.398557	0.000117	36.96	15.80	12.680	0.151
H I	1215.67	4135.61	2.401921	0.000032	9.65	4.45	12.367	0.146
H I	1025.72	4135.94	3.032231	0.000004	24.41	0.48	13.507	0.010
H I	1215.67	4137.08	2.403128	0.000060	40.59	7.56	12.861	0.069
H I	1215.67	4141.37	2.406656	0.000023	48.68	2.75	13.545	0.022
Fe II	1143.23	4143.49	2.624384	0.000023	15.00	3.39	12.760	0.077
Fe II	1143.23	4144.41	2.625190	0.000003	22.47	0.29	14.785	0.008
H I	1215.67	4144.78	2.409458	0.000064	64.63	8.15	13.338	0.048
Fe II	1143.23	4144.94	2.625649	0.000005	6.31	1.02	14.284	0.122
Fe II	1143.23	4145.09	2.625782	0.000177	12.73	7.26	13.637	0.492
Fe II	1143.23	4145.26	2.625936	0.000005	3.26	1.28	13.256	0.156
H I	1215.67	4146.15	2.410590	0.000027	21.77	3.61	12.907	0.059
Si II	1190.42	4146.99	2.483654	0.000009	13.65	0.94	13.072	0.029
Si II	1190.42	4147.24	2.483862	0.000007	4.78	1.35	12.479	0.096
Si II	1190.42	4147.49	2.484076	0.000003	6.96	0.40	13.032	0.016
Fe II	1144.94	4149.70	2.624384	0.000023	15.00	3.39	12.760	0.077
Fe II	1144.94	4150.62	2.625190	0.000003	22.47	0.29	14.785	0.008
Fe II	1144.94	4151.14	2.625649	0.000005	6.31	1.02	14.284	0.122
Fe II	1144.94	4151.30	2.625782	0.000177	12.73	7.26	13.637	0.492
Fe II	1144.94	4151.47	2.625936	0.000005	3.26	1.28	13.256	0.156
H I	1025.72	4151.03	3.046940	0.000027	16.98	1.50	13.034	0.105
H I	1025.72	4151.39	3.047284	0.000032	19.38	2.20	13.112	0.092
H I	1215.67	4153.39	2.416549	0.000005	26.80	0.85	14.403	0.046
H I	1025.72	4153.87	3.049704	0.000003	29.99	0.20	13.710	0.005
Si II	1193.29	4157.00	2.483654	0.000009	13.65	0.94	13.072	0.029
H I	1215.67	4157.15	2.419643	0.000028	11.36	3.48	12.705	0.108
Si II	1193.29	4157.25	2.483862	0.000007	4.78	1.35	12.479	0.096
Si II	1193.29	4157.51	2.484076	0.000003	6.96	0.40	13.032	0.016
H I	1215.67	4159.21	2.421338	0.000048	53.48	5.80	13.186	0.042
H I	1215.67	4163.24	2.424646	0.000133	55.40	20.99	12.698	0.140
H I	1215.67	4165.39	2.426421	0.000149	67.03	21.44	12.914	0.110
H I	1215.67	4166.94	2.427693	0.000034	12.09	4.61	12.465	0.138
H I	1215.67	4168.50	2.428980	0.000089	56.12	11.25	13.005	0.074
H I	1215.67	4170.77	2.430846	0.000014	28.76	1.44	14.020	0.026
H I	1215.67	4171.74	2.431646	0.000013	24.80	1.78	14.056	0.036
H I	1215.67	4173.02	2.432695	0.000105	74.20	17.54	13.416	0.084
H I	1215.67	4174.61	2.434004	0.000018	21.58	2.57	13.177	0.052
H I	1215.67	4175.46	2.434698	0.000010	22.88	1.22	13.469	0.019
P II	1152.82	4179.22	2.625222	0.000017	10.77	2.11	12.935	0.068
H I	1215.67	4180.73	2.439041	0.000006	45.78	1.10	14.624	0.034
H I	1215.67	4186.61	2.443875	0.000009	24.76	1.06	13.396	0.017
H I	1215.67	4188.14	2.445136	0.000038	39.55	4.94	13.017	0.045
H I	1215.67	4189.66	2.446382	0.000018	34.24	2.28	13.238	0.024
H I	1215.67	4191.17	2.447628	0.000042	24.87	5.48	12.600	0.078
H I	1215.67	4192.16	2.448438	0.000023	20.24	3.09	12.773	0.056
H I	1215.67	4193.29	2.449366	0.000146	39.77	16.47	12.606	0.259
H I	1215.67	4194.60	2.450448	0.000137	61.38	37.36	12.805	0.228
H I	1215.67	4195.99	2.451590	0.000058	28.44	7.12	12.674	0.133
Si III	1206.50	4199.36	2.480619	0.000006	8.51	0.75	12.435	0.028
Si III	1206.50	4199.65	2.480854	0.000006	6.34	0.78	12.293	0.034
H I	1215.67	4200.81	2.455554	0.000023	11.25	3.09	12.340	0.091

Table 4. Absorption line parameter list

ID	λ_{rest}	λ_{obs}	z	σ_z	b	σ_b	$\text{Log}N$	$\sigma_{\text{Log}N}$
H I	1215.67	4201.59	2.456196	0.000007	20.86	0.84	13.364	0.016
Si III	1206.50	4203.22	2.483818	0.000025	13.50	0.79	14.224	0.295
Si III	1206.50	4203.74	2.484244	0.000041	20.32	2.22	13.278	0.097
H I	1215.67	4207.29	2.460888	0.000051	50.90	6.16	13.084	0.045
H I	1215.67	4209.72	2.462880	0.000033	23.53	4.06	12.758	0.063
H I	1215.67	4211.76	2.464566	0.000006	30.67	0.78	14.123	0.021
H I	1215.67	4214.71	2.466985	0.000015	23.07	1.72	13.328	0.030
H I	1215.67	4217.25	2.469076	0.000060	53.40	7.81	13.219	0.052
H I	1215.67	4219.01	2.470529	0.000023	32.63	2.49	13.823	0.030
H I	1215.67	4219.84	2.471210	0.000026	22.25	2.58	13.431	0.058
H I	1215.67	4229.09	2.478820	0.000301	100.00	28.49	13.280	0.141
H I	1215.67	4231.37	2.480691	0.000009	18.62	1.84	15.088	0.288
H I	1215.67	4232.20	2.481372	0.000145	100.00	16.89	13.988	0.063
H I	1215.67	4234.24	2.483056	0.000048	39.33	4.71	14.801	0.165
H I	1215.67	4236.21	2.484674	0.000073	84.35	12.28	14.694	0.038
H I	1215.67	4238.21	2.486319	0.000016	21.96	2.72	15.256	0.350
H I	1215.67	4239.29	2.487205	0.000050	46.66	4.51	13.653	0.046
H I	1215.67	4244.90	2.491824	0.000042	19.82	5.42	12.519	0.098
H I	1215.67	4250.77	2.496646	0.000007	21.78	0.80	13.569	0.017
H I	1215.67	4252.47	2.498043	0.000018	34.88	2.14	13.336	0.024
H I	1215.67	4254.49	2.499703	0.000026	27.36	2.46	13.547	0.041
H I	1215.67	4255.17	2.500261	0.000013	20.03	1.19	13.737	0.031
H I	1215.67	4257.69	2.502333	0.000024	20.67	2.68	13.090	0.052
H I	1215.67	4258.96	2.503379	0.000009	37.42	1.40	14.557	0.048
H I	1215.67	4268.38	2.511126	0.000022	23.03	2.67	13.133	0.046
H I	1215.67	4269.76	2.512266	0.000066	51.96	8.68	13.138	0.058
H I	1215.67	4273.74	2.515535	0.000081	52.65	11.12	12.949	0.079
H I	1215.67	4282.77	2.522968	0.000041	29.73	4.74	12.897	0.060
H I	1215.67	4284.49	2.524385	0.000037	23.69	4.67	12.736	0.070
H I	1215.67	4285.88	2.525523	0.000013	27.70	1.57	13.395	0.021
H I	1215.67	4287.25	2.526649	0.000006	30.35	1.04	14.342	0.034
H I	1215.67	4288.74	2.527875	0.000027	37.67	3.31	13.682	0.035
H I	1215.67	4289.78	2.528730	0.000035	34.58	3.02	13.499	0.046
H I	1215.67	4294.48	2.532599	0.000022	15.58	2.70	12.612	0.061
H I	1215.67	4295.63	2.533542	0.000071	32.00	8.87	12.521	0.100
H I	1215.67	4297.89	2.535407	0.000040	37.24	4.83	12.881	0.048
H I	1215.67	4301.71	2.538543	0.000006	41.54	0.71	14.068	0.010
H I	1215.67	4305.52	2.541685	0.000006	7.79	0.72	12.875	0.031
H I	1215.67	4308.59	2.544209	0.000067	25.23	8.37	12.554	0.122
H I	1215.67	4309.40	2.544876	0.000043	21.98	5.87	12.668	0.094
Si II	1190.42	4314.51	2.624365	0.000003	10.63	0.28	13.410	0.012
Si II	1190.42	4314.81	2.624617	0.000003	3.27	0.33	13.076	0.025
H I	1215.67	4315.23	2.549668	0.000061	58.07	3.40	13.940	0.075
Si II	1190.42	4315.59	2.625274	0.000007	16.77	0.28	16.655	0.040
Si II	1190.42	4316.31	2.625883	0.000009	9.60	0.57	14.167	0.040
Si II	1190.42	4316.70	2.626211	0.000009	8.58	1.01	12.602	0.046
H I	1215.67	4318.67	2.552497	0.000011	23.42	1.32	13.497	0.026
H I	1215.67	4319.78	2.553408	0.000053	73.41	30.83	12.815	0.160
H I	1215.67	4321.62	2.554927	0.000012	6.80	1.63	12.616	0.073
H I	1215.67	4322.77	2.555873	0.000077	34.34	9.37	12.734	0.101
H I	1215.67	4323.90	2.556799	0.000041	9.23	5.38	12.206	0.188
Si II	1193.29	4324.92	2.624365	0.000003	10.63	0.28	13.410	0.012
Si II	1193.29	4325.22	2.624617	0.000003	3.27	0.33	13.076	0.025
Si II	1193.29	4326.01	2.625274	0.000007	16.77	0.28	16.655	0.040
Si II	1193.29	4326.73	2.625883	0.000009	9.60	0.57	14.167	0.040
Si II	1193.29	4327.12	2.626211	0.000009	8.58	1.01	12.602	0.046
H I	1215.67	4327.67	2.559904	0.000047	17.53	5.85	12.485	0.122
H I	1215.67	4333.49	2.564688	0.000029	22.84	3.53	12.833	0.056
H I	1215.67	4336.43	2.567108	0.000006	21.76	0.62	13.805	0.018
H I	1215.67	4339.68	2.569779	0.000004	32.74	0.85	14.968	0.061
H I	1215.67	4344.23	2.573525	0.000020	9.78	2.56	12.446	0.094
H I	1215.67	4344.91	2.574084	0.000007	24.55	0.83	13.643	0.013
H I	1215.67	4347.31	2.576061	0.000040	45.92	5.05	13.117	0.040

Table 4. Absorption line parameter list

ID	λ_{rest}	λ_{obs}	z	σ_z	b	σ_b	$\text{Log}N$	$\sigma_{\text{Log}N}$
N I	1199.55	4348.59	2.625185	0.000013	19.12	1.51	14.704	0.072
N I	1199.55	4348.82	2.625376	0.000041	33.77	2.34	14.387	0.153
N I	1199.55	4349.12	2.625624	0.000006	7.64	0.74	14.318	0.050
N I	1200.22	4351.04	2.625185	0.000013	19.12	1.51	14.704	0.072
N I	1200.22	4351.27	2.625376	0.000041	33.77	2.34	14.387	0.153
N I	1200.22	4351.56	2.625624	0.000006	7.64	0.74	14.318	0.050
H I	1215.67	4352.60	2.580412	0.000021	36.93	1.71	13.831	0.032
N I	1200.71	4352.80	2.625185	0.000013	19.12	1.51	14.704	0.072
N I	1200.71	4353.03	2.625376	0.000041	33.77	2.34	14.387	0.153
N I	1200.71	4353.33	2.625624	0.000006	7.64	0.74	14.318	0.050
H I	1215.67	4356.04	2.583239	0.000044	74.97	4.55	13.522	0.031
H I	1215.67	4356.39	2.583530	0.000016	19.35	2.33	13.071	0.063
H I	1215.67	4359.51	2.586095	0.000088	100.00	12.36	13.238	0.049
H I	1215.67	4363.89	2.589694	0.000106	100.00	14.81	13.161	0.059
H I	1215.67	4366.49	2.591832	0.000012	29.51	1.41	13.449	0.020
H I	1215.67	4368.80	2.593736	0.000098	94.39	12.32	13.310	0.051
Si III	1206.50	4369.47	2.621601	0.000007	8.18	0.78	12.466	0.035
H I	1215.67	4372.33	2.596643	0.000244	26.50	16.01	12.760	0.483
Si III	1206.50	4372.66	2.624248	0.000012	4.97	2.14	13.591	0.921
Si III	1206.50	4373.77	2.625171	0.000023	40.88	10.62	14.370	0.319
Si III	1206.50	4375.01	2.626200	0.000016	9.76	1.69	14.128	0.387
H I	1215.67	4377.77	2.601116	0.000019	14.87	2.28	12.932	0.057
H I	1215.67	4381.85	2.604468	0.000011	38.78	1.40	14.296	0.030
H I	1215.67	4383.41	2.605754	0.000028	32.69	4.01	13.365	0.041
H I	1215.67	4384.67	2.606787	0.000008	23.10	1.31	14.277	0.071
H I	1215.67	4387.39	2.609027	0.000085	54.05	10.47	13.153	0.083
H I	1215.67	4389.35	2.610643	0.000044	13.70	5.54	12.595	0.138
H I	1215.67	4390.36	2.611472	0.000016	17.13	1.69	13.687	0.049
Si II	1260.42	4390.88	2.483654	0.000009	13.65	0.94	13.072	0.029
Si II	1260.42	4391.14	2.483862	0.000007	4.78	1.35	12.479	0.096
Si II	1260.42	4391.41	2.484076	0.000003	6.96	0.40	13.032	0.016
H I	1215.67	4393.48	2.614033	0.000017	24.21	2.38	14.146	0.103
H I	1215.67	4407.51	2.625579	0.000049	78.50	46.63	20.761	0.007
H I	1215.67	4425.57	2.640430	0.000039	14.96	4.62	12.802	0.113
H I	1215.67	4428.98	2.643236	0.000047	19.01	5.62	12.739	0.110
H I	1215.67	4431.24	2.645099	0.000016	22.89	1.85	13.374	0.033
H I	1215.67	4433.34	2.646828	0.000060	57.20	7.06	13.267	0.049
H I	1215.67	4436.10	2.649093	0.000063	40.77	7.51	12.902	0.072
H I	1215.67	4439.03	2.651502	0.000052	64.59	5.54	13.415	0.039
H I	1215.67	4440.79	2.652952	0.000080	24.28	13.30	12.479	0.348
H I	1215.67	4441.98	2.653930	0.000302	100.00	29.02	13.158	0.135
H I	1215.67	4445.36	2.656714	0.000069	37.86	8.71	12.693	0.087
H I	1215.67	4447.41	2.658396	0.000095	47.04	12.19	12.662	0.100
H I	1215.67	4449.50	2.660116	0.000078	48.30	9.62	12.850	0.083
H I	1215.67	4452.20	2.662337	0.000149	100.00	25.36	12.995	0.091
H I	1215.67	4454.48	2.664216	0.000016	14.11	2.10	13.332	0.086
H I	1215.67	4454.69	2.664383	0.000013	38.57	1.26	13.875	0.023
H I	1215.67	4456.40	2.665794	0.000049	43.14	7.70	12.926	0.062
H I	1215.67	4457.79	2.666937	0.000054	29.58	7.43	12.631	0.094
H I	1215.67	4459.12	2.668033	0.000016	30.80	1.75	13.550	0.022
H I	1215.67	4460.01	2.668760	0.000087	26.55	13.00	12.622	0.286
H I	1215.67	4461.30	2.669828	0.000011	23.93	2.00	13.310	0.055
H I	1215.67	4462.13	2.670511	0.000315	100.00	29.25	13.169	0.154
H I	1215.67	4463.87	2.671936	0.000025	13.83	3.57	12.427	0.112
H I	1215.67	4465.44	2.673230	0.000023	20.58	2.78	12.819	0.048
C IV	1548.20	4466.27	1.884823	0.000002	5.23	0.30	13.851	0.044
H I	1215.67	4466.60	2.674188	0.000046	29.62	4.22	12.945	0.065
C IV	1550.77	4473.70	1.884823	0.000002	5.23	0.30	13.851	0.044
Fe II	1144.94	4476.93	2.910193	0.000003	10.10	0.28	13.658	0.010
H I	1215.67	4477.15	2.682861	0.000072	44.64	7.38	13.220	0.048
H I	1215.67	4478.39	2.683881	0.000072	35.44	7.04	12.968	0.098
H I	1215.67	4480.43	2.685562	0.000065	32.17	8.31	12.665	0.089
Si II	1526.71	4481.13	1.935161	0.000005	1.66	2.06	13.059	0.179

Table 4. Absorption line parameter list

ID	λ_{rest}	λ_{obs}	z	σ_z	b	σ_b	$\text{Log}N$	$\sigma_{\text{Log}N}$
Si II	1526.71	4481.28	1.935259	0.000034	11.16	3.95	13.086	0.161
H I	1215.67	4483.04	2.687711	0.000161	78.46	23.65	12.863	0.100
H I	1215.67	4485.30	2.689567	0.000045	21.08	3.30	13.850	0.130
H I	1215.67	4485.92	2.690076	0.000025	53.35	1.26	14.325	0.030
H I	1215.67	4488.50	2.692196	0.000062	34.84	6.63	13.230	0.083
H I	1215.67	4489.50	2.693025	0.000040	26.24	3.18	14.058	0.076
N V	1238.82	4490.14	2.624522	0.000007	6.64	0.90	13.246	0.039
H I	1215.67	4490.47	2.693822	0.000036	30.94	1.64	14.509	0.076
N V	1238.82	4491.94	2.625976	0.000026	14.29	3.23	12.827	0.085
H I	1215.67	4493.46	2.696279	0.000068	63.01	9.53	12.985	0.051
Mg II	1239.93	4495.10	2.625286	0.000016	26.73	3.17	15.502	0.082
Mg II	1239.93	4495.55	2.625646	0.000003	8.28	0.62	15.319	0.091
H I	1215.67	4495.89	2.698284	0.000011	28.41	1.22	13.584	0.018
Mg II	1240.40	4496.80	2.625286	0.000016	26.73	3.17	15.502	0.082
Mg II	1240.40	4497.25	2.625646	0.000003	8.28	0.62	15.319	0.091
H I	1215.67	4498.31	2.700265	0.000016	31.99	1.97	13.193	0.025
H I	1215.67	4500.06	2.701707	0.000037	26.43	6.39	12.677	0.153
H I	1215.67	4501.11	2.702570	0.000158	100.00	14.04	13.217	0.069
H I	1215.67	4503.10	2.704212	0.000037	12.88	4.92	12.134	0.150
N V	1242.80	4504.57	2.624522	0.000007	6.64	0.90	13.246	0.039
N V	1242.80	4506.38	2.625976	0.000026	14.29	3.23	12.827	0.085
H I	1215.67	4509.44	2.709421	0.000004	38.40	0.78	15.040	0.048
H I	1215.67	4512.95	2.712308	0.000022	35.05	2.58	13.013	0.027
H I	1215.67	4514.16	2.713305	0.000011	13.99	1.63	13.035	0.088
H I	1215.67	4514.78	2.713818	0.000019	35.26	2.51	13.665	0.027
H I	1215.67	4516.55	2.715271	0.000004	37.27	0.91	14.805	0.039
H I	1215.67	4518.45	2.716834	0.000010	38.43	1.31	13.537	0.012
H I	1215.67	4520.13	2.718220	0.000014	35.32	1.90	13.327	0.031
H I	1215.67	4522.04	2.719789	0.000158	100.00	25.88	13.025	0.089
H I	1215.67	4525.26	2.722435	0.000110	65.97	14.82	12.824	0.089
H I	1215.67	4528.79	2.725343	0.000281	100.00	23.54	13.412	0.123
H I	1215.67	4530.20	2.726498	0.000008	36.73	1.30	14.321	0.022
H I	1215.67	4531.81	2.727829	0.000133	46.96	15.03	12.666	0.138
S II	1250.58	4533.73	2.625284	0.000007	17.78	0.91	14.992	0.022
S II	1250.58	4534.16	2.625633	0.000006	6.68	0.75	14.673	0.053
S II	1250.58	4534.40	2.625820	0.000039	10.48	3.69	14.093	0.173
O I	1302.17	4536.31	2.483654	0.000000	18.09	0.00	13.698	0.040
O I	1302.17	4536.86	2.484076	0.000000	9.22	0.00	12.903	0.160
H I	1215.67	4538.76	2.733545	0.000008	26.15	0.86	13.853	0.014
H I	1215.67	4539.61	2.734239	0.000013	18.92	1.32	13.316	0.028
C IV	1548.20	4541.89	1.933663	0.000005	8.01	0.77	13.064	0.033
H I	1215.67	4543.60	2.737520	0.000728	77.36	58.69	12.841	0.411
Si II	1304.37	4543.98	2.483654	0.000009	13.65	0.94	13.072	0.029
C IV	1548.19	4544.11	1.935102	0.000004	12.96	0.83	13.706	0.037
Si II	1304.37	4544.25	2.483862	0.000007	4.78	1.35	12.479	0.096
Si II	1304.37	4544.53	2.484076	0.000003	6.96	0.40	13.032	0.016
C IV	1548.20	4544.70	1.935480	0.000009	12.12	1.87	13.258	0.096
C IV	1548.20	4545.20	1.935805	0.000007	13.40	1.17	13.562	0.048
S II	1253.81	4545.42	2.625284	0.000007	17.78	0.91	14.992	0.022
C IV	1548.20	4545.72	1.936137	0.000005	8.05	0.86	13.437	0.048
S II	1253.81	4545.86	2.625633	0.000006	6.68	0.75	14.673	0.053
S II	1253.81	4546.10	2.625820	0.000039	10.48	3.69	14.093	0.173
C IV	1548.20	4546.88	1.936890	0.000008	6.05	1.45	12.637	0.070
C IV	1550.77	4549.44	1.933663	0.000005	8.01	0.77	13.064	0.033
H I	1215.67	4551.32	2.743878	0.000025	37.42	1.16	14.784	0.058
C IV	1550.77	4551.67	1.935102	0.000004	12.96	0.83	13.706	0.037
C IV	1550.77	4552.26	1.935480	0.000009	12.12	1.87	13.258	0.096
H I	1215.67	4552.56	2.744891	0.000127	47.28	26.75	13.676	0.414
C IV	1550.77	4552.76	1.935805	0.000007	13.40	1.17	13.562	0.048
C IV	1550.77	4553.28	1.936137	0.000005	8.05	0.86	13.437	0.048
H I	1215.67	4553.74	2.745866	0.001025	66.64	58.89	13.222	0.721
C IV	1550.77	4554.44	1.936890	0.000008	6.05	1.45	12.637	0.070
H I	1215.67	4554.72	2.746675	0.000028	16.94	5.21	12.671	0.211

Table 4. Absorption line parameter list

ID	λ_{rest}	λ_{obs}	z	σ_z	b	σ_b	$\text{Log}N$	$\sigma_{\text{Log}N}$
H I	1215.67	4555.48	2.747295	0.000030	8.99	5.44	12.065	0.286
H I	1215.67	4556.82	2.748399	0.000009	24.56	1.02	13.374	0.020
H I	1215.67	4558.45	2.749737	0.000050	70.61	4.54	13.675	0.031
H I	1215.67	4558.90	2.750113	0.000010	12.46	1.00	13.333	0.044
H I	1215.67	4559.37	2.750500	0.000056	22.11	6.56	12.911	0.171
H I	1215.67	4560.90	2.751753	0.000003	20.84	0.41	13.904	0.012
H I	1215.67	4563.09	2.753555	0.000120	100.00	19.56	13.040	0.064
H I	1215.67	4564.74	2.754910	0.000004	2.09	0.74	12.770	0.095
H I	1215.67	4565.32	2.755393	0.000006	25.99	0.81	13.910	0.011
S II	1259.52	4566.12	2.625284	0.000007	17.78	0.91	14.992	0.022
S II	1259.52	4566.56	2.625633	0.000006	6.68	0.75	14.673	0.053
H I	1215.67	4566.73	2.756550	0.000044	37.13	3.38	13.369	0.049
S II	1259.52	4566.79	2.625820	0.000039	10.48	3.69	14.093	0.173
Si II	1260.42	4568.23	2.624365	0.000003	10.63	0.28	13.410	0.012
Si II	1260.42	4568.55	2.624617	0.000003	3.27	0.33	13.076	0.025
Si II	1260.42	4569.38	2.625274	0.000007	16.77	0.28	16.655	0.040
Si II	1260.42	4570.15	2.625883	0.000009	9.60	0.57	14.167	0.040
Si II	1260.42	4570.56	2.626211	0.000009	8.58	1.01	12.602	0.046
H I	1215.67	4571.89	2.760796	0.000008	33.70	0.94	13.558	0.010
H I	1215.67	4573.22	2.761886	0.000011	33.04	1.27	13.374	0.014
H I	1215.67	4576.39	2.764499	0.000175	98.17	20.89	13.046	0.089
H I	1215.67	4579.60	2.767135	0.000081	96.57	14.68	13.427	0.062
H I	1215.67	4581.01	2.768299	0.000018	24.13	2.93	12.933	0.074
H I	1215.67	4583.43	2.770287	0.000048	100.00	5.74	13.488	0.021
H I	1215.67	4587.06	2.773273	0.000012	37.74	1.36	13.356	0.014
H I	1215.67	4590.84	2.776380	0.000176	100.00	14.30	13.360	0.073
H I	1215.67	4592.24	2.777534	0.000004	28.48	0.88	14.566	0.041
H I	1215.67	4593.76	2.778787	0.000011	18.93	1.36	13.132	0.027
H I	1215.67	4594.54	2.779425	0.000031	17.23	4.20	12.671	0.090
H I	1215.67	4595.43	2.780159	0.000006	25.86	0.73	14.016	0.015
H I	1215.67	4596.61	2.781132	0.000048	22.44	6.88	12.429	0.106
H I	1215.67	4602.52	2.785990	0.000017	44.32	1.69	13.770	0.015
H I	1215.67	4603.92	2.787142	0.000006	28.33	0.85	14.527	0.042
H I	1215.67	4608.80	2.791154	0.000048	29.18	5.67	12.592	0.069
H I	1215.67	4610.29	2.792382	0.000050	33.26	4.98	12.948	0.091
H I	1215.67	4612.09	2.793865	0.000339	59.49	18.90	13.818	0.272
H I	1215.67	4613.78	2.795255	0.000019	46.91	1.36	16.186	0.101
H I	1215.67	4616.62	2.797589	0.000070	43.92	9.37	13.028	0.082
H I	1215.67	4617.54	2.798348	0.000006	21.57	0.57	13.750	0.015
H I	1215.67	4622.08	2.802077	0.000052	59.83	6.30	12.915	0.037
H I	1215.67	4623.76	2.803462	0.000004	21.64	0.41	13.617	0.008
H I	1215.67	4626.44	2.805671	0.000007	15.54	0.82	12.911	0.019
H I	1215.67	4632.63	2.810756	0.000017	24.98	1.94	12.793	0.029
H I	1215.67	4634.24	2.812082	0.000008	22.85	0.90	13.097	0.015
H I	1215.67	4638.98	2.815980	0.000055	37.55	6.05	12.787	0.063
Si III	1206.50	4640.16	2.845968	0.000009	12.75	1.21	12.484	0.063
Si III	1206.50	4640.61	2.846340	0.000043	44.16	4.73	12.776	0.052
Si III	1206.50	4640.67	2.846386	0.000009	8.34	1.60	12.156	0.103
Si III	1206.50	4641.87	2.847381	0.000002	5.59	0.33	12.848	0.036
Si III	1206.50	4642.24	2.847690	0.000064	33.73	5.54	12.258	0.077
Si III	1206.50	4644.01	2.849158	0.000017	5.23	2.63	11.465	0.146
Si III	1206.50	4644.56	2.849617	0.000012	4.61	0.54	15.786	0.032
Si III	1206.50	4644.89	2.849887	0.000017	6.25	1.29	12.748	0.101
H I	1215.67	4646.17	2.821894	0.000034	35.12	4.19	12.854	0.042
H I	1215.67	4647.89	2.823315	0.000016	34.95	1.90	13.136	0.019
C II	1334.53	4649.10	2.483693	0.000014	15.95	2.10	13.828	0.152
H I	1215.67	4649.51	2.824646	0.000125	29.77	5.95	13.276	0.200
C II	1334.53	4649.62	2.484077	0.000003	4.11	0.57	13.571	0.044
H I	1215.67	4652.09	2.826766	0.000033	51.40	3.86	13.140	0.027
Si II	1190.42	4654.10	2.909643	0.000003	8.10	0.50	12.476	0.035
Si II	1190.42	4654.71	2.910154	0.000011	31.31	1.33	13.266	0.016
Si II	1190.42	4654.72	2.910164	0.000003	7.79	0.22	14.011	0.034
Si II	1190.42	4654.87	2.910289	0.000028	11.42	0.88	13.331	0.132

Table 4. Absorption line parameter list

ID	λ_{rest}	λ_{obs}	z	σ_z	b	σ_b	$\text{Log}N$	$\sigma_{\text{Log}N}$
Si II	1190.42	4655.47	2.910793	0.000002	6.02	0.30	12.414	0.018
Si II	1190.42	4655.85	2.911111	0.000001	10.40	0.19	12.853	0.006
Si II	1190.42	4656.21	2.911411	0.000011	3.70	1.87	11.272	0.095
H I	1215.67	4657.55	2.831258	0.000031	16.23	4.15	12.539	0.119
H I	1215.67	4658.32	2.831891	0.000044	84.19	3.93	13.537	0.020
H I	1215.67	4662.54	2.835365	0.000005	63.11	1.10	15.715	0.056
Si II	1193.29	4665.34	2.909643	0.000003	8.10	0.50	12.476	0.035
Si II	1193.29	4665.95	2.910154	0.000011	31.31	1.33	13.266	0.016
Si II	1193.29	4665.96	2.910164	0.000003	7.79	0.22	14.011	0.034
Si II	1193.29	4666.11	2.910289	0.000028	11.42	0.88	13.331	0.132
H I	1215.67	4666.38	2.838523	0.000008	41.59	0.94	14.290	0.023
Si II	1193.29	4666.71	2.910793	0.000002	6.02	0.30	12.414	0.018
Si II	1193.29	4667.09	2.911111	0.000001	10.40	0.19	12.853	0.006
Si II	1193.29	4667.45	2.911411	0.000011	3.70	1.87	11.272	0.095
H I	1215.67	4668.10	2.839941	0.000014	22.80	1.89	13.121	0.038
H I	1215.67	4669.55	2.841133	0.000040	24.84	6.31	12.680	0.163
H I	1215.67	4670.23	2.841690	0.000132	91.92	9.92	13.311	0.064
H I	1215.67	4674.35	2.845081	0.000024	23.22	1.49	13.669	0.049
H I	1215.67	4677.68	2.847815	0.000013	62.87	0.62	18.253	0.062
H I	1215.67	4681.74	2.851154	0.000048	68.28	5.49	13.334	0.040
H I	1215.67	4684.58	2.853494	0.000025	21.66	2.90	12.589	0.047
H I	1215.67	4688.20	2.856475	0.000025	24.58	2.75	12.640	0.041
H I	1215.67	4689.84	2.857824	0.000011	24.16	0.89	13.541	0.017
H I	1215.67	4690.50	2.858367	0.000041	20.14	3.39	12.766	0.093
H I	1215.67	4692.23	2.859790	0.000025	36.93	2.82	13.035	0.028
H I	1215.67	4693.60	2.860913	0.000011	36.15	1.22	13.413	0.012
H I	1215.67	4695.37	2.862372	0.000032	21.76	3.76	12.452	0.061
H I	1215.67	4697.06	2.863758	0.000003	39.98	0.46	14.409	0.011
H I	1215.67	4700.24	2.866377	0.000301	100.00	29.90	12.955	0.142
H I	1215.67	4702.84	2.868515	0.000083	81.04	8.78	13.333	0.060
H I	1215.67	4704.68	2.870028	0.000029	20.18	3.98	12.461	0.089
H I	1215.67	4705.93	2.871052	0.000008	34.30	1.00	13.531	0.015
H I	1215.67	4708.48	2.873153	0.000684	100.00	44.32	13.342	0.318
H I	1215.67	4709.78	2.874219	0.000007	51.04	1.69	14.297	0.030
H I	1215.67	4712.41	2.876386	0.000018	28.92	3.50	13.305	0.124
H I	1215.67	4713.19	2.877031	0.000082	62.05	4.64	13.710	0.055
Si III	1206.50	4717.07	2.909713	0.000009	7.66	0.61	12.934	0.067
Si III	1206.50	4717.67	2.910208	0.000011	19.68	3.44	13.701	0.090
Si III	1206.50	4719.01	2.911317	0.000031	28.25	5.81	14.503	0.343
O I	1302.17	4720.72	2.625274	0.000000	22.22	0.00	18.090	0.153
O I	1302.17	4721.94	2.626211	0.000000	11.36	0.00	13.259	0.388
H I	1215.67	4722.33	2.884545	0.000018	23.95	1.79	13.604	0.031
H I	1215.67	4723.31	2.885351	0.000015	16.85	1.99	12.948	0.042
H I	1215.67	4724.02	2.885940	0.000052	19.75	7.13	12.464	0.125
H I	1215.67	4725.32	2.887010	0.000006	34.67	0.64	14.003	0.010
Si II	1304.37	4727.52	2.624365	0.000003	10.63	0.28	13.410	0.012
Si II	1304.37	4727.85	2.624617	0.000003	3.27	0.33	13.076	0.025
Si II	1304.37	4728.70	2.625274	0.000007	16.77	0.28	16.655	0.040
Si II	1304.37	4729.50	2.625883	0.000009	9.60	0.57	14.167	0.040
Si II	1304.37	4729.92	2.626211	0.000009	8.58	1.01	12.602	0.046
H I	1215.67	4735.73	2.895573	0.000004	26.07	0.44	13.997	0.011
H I	1215.67	4737.49	2.897021	0.000005	43.82	0.59	14.245	0.008
H I	1215.67	4739.68	2.898819	0.000042	18.95	4.86	12.365	0.094
H I	1215.67	4741.29	2.900141	0.000012	43.68	1.12	13.834	0.012
H I	1215.67	4743.22	2.901728	0.000024	67.04	2.80	13.748	0.016
H I	1215.67	4746.20	2.904185	0.000037	29.01	4.24	12.913	0.068
H I	1215.67	4747.93	2.905605	0.000050	33.29	6.10	13.106	0.090
H I	1215.67	4753.47	2.910160	0.000031	58.77	1.71	19.795	0.006
H I	1215.67	4760.20	2.915699	0.000038	67.99	2.60	17.021	0.205
H I	1215.67	4763.77	2.918631	0.000011	24.29	1.09	13.496	0.019
H I	1215.67	4766.71	2.921050	0.000033	22.35	3.80	12.549	0.065
H I	1215.67	4768.45	2.922484	0.000010	14.87	1.15	12.841	0.028
H I	1215.67	4774.49	2.927459	0.000016	34.91	1.62	13.320	0.018

Table 4. Absorption line parameter list

ID	λ_{rest}	λ_{obs}	z	σ_z	b	σ_b	$\text{Log}N$	$\sigma_{\text{Log}N}$
Ni II	1317.22	4775.07	2.625111	0.000296	31.35	10.65	13.310	0.527
Ni II	1317.22	4775.30	2.625286	0.000016	17.20	3.17	13.532	0.275
Ni II	1317.22	4775.77	2.625646	0.000003	5.33	0.62	13.168	0.063
Ni II	1317.22	4776.04	2.625847	0.000046	15.20	4.54	12.921	0.159
H I	1215.67	4777.80	2.930174	0.000005	29.71	0.52	14.054	0.010
H I	1215.67	4778.92	2.931097	0.000071	25.10	10.02	12.333	0.150
H I	1215.67	4781.16	2.932938	0.000004	23.84	0.45	14.116	0.018
H I	1215.67	4782.55	2.934086	0.000008	19.21	0.90	13.261	0.018
H I	1215.67	4783.67	2.935006	0.000018	35.25	2.07	13.275	0.020
H I	1215.67	4786.47	2.937308	0.000245	31.05	11.80	13.087	0.344
H I	1215.67	4786.99	2.937736	0.000011	19.38	1.29	14.035	0.041
H I	1215.67	4787.98	2.938546	0.000021	10.98	3.37	12.762	0.213
H I	1215.67	4788.63	2.939084	0.000072	55.16	10.13	13.669	0.085
H I	1215.67	4788.75	2.939180	0.000015	18.78	2.44	13.562	0.098
H I	1215.67	4790.48	2.940604	0.000070	60.27	5.99	13.557	0.050
H I	1215.67	4791.40	2.941360	0.000014	13.47	2.01	12.801	0.076
H I	1215.67	4794.04	2.943531	0.000004	42.61	0.83	15.108	0.045
H I	1215.67	4795.69	2.944895	0.000024	8.63	3.21	12.179	0.140
H I	1215.67	4796.68	2.945706	0.000061	34.04	4.18	13.427	0.076
H I	1215.67	4798.25	2.946998	0.000008	36.81	2.65	15.405	0.152
H I	1215.67	4799.71	2.948196	0.000046	21.45	2.72	13.149	0.103
H I	1215.67	4803.11	2.950996	0.000013	28.53	1.46	13.164	0.019
H I	1215.67	4804.14	2.951839	0.000020	27.57	2.27	12.951	0.031
H I	1215.67	4810.56	2.957122	0.000026	29.24	2.88	12.681	0.036
H I	1215.67	4812.56	2.958766	0.000007	22.39	0.73	13.120	0.012
H I	1215.67	4814.85	2.960656	0.000017	19.46	1.84	12.593	0.034
H I	1215.67	4817.96	2.963207	0.000018	26.26	1.92	12.753	0.027
H I	1215.67	4819.29	2.964301	0.000020	14.30	2.21	12.315	0.053
H I	1215.67	4821.75	2.966330	0.000013	19.25	1.38	12.705	0.026
H I	1215.67	4826.06	2.969876	0.000026	47.08	0.92	14.562	0.031
H I	1215.67	4827.11	2.970740	0.000022	20.21	1.14	14.083	0.063
H I	1215.67	4828.55	2.971925	0.000038	62.74	4.39	13.147	0.025
H I	1215.67	4830.78	2.973757	0.000032	15.02	3.62	12.103	0.084
H I	1215.67	4831.74	2.974549	0.000022	13.53	2.46	12.208	0.062
C II	1334.53	4833.14	2.621597	0.000004	3.19	0.60	12.755	0.031
H I	1215.67	4834.48	2.976798	0.000018	17.31	2.06	12.469	0.041
H I	1215.67	4836.24	2.978247	0.000115	22.92	9.56	12.377	0.200
C II	1334.53	4836.90	2.624411	0.000012	16.07	1.02	14.296	0.045
C II	1334.53	4838.15	2.625353	0.000012	36.62	0.77	15.650	0.043
C II*	1335.71	4842.31	2.625274	0.000018	5.02	2.65	12.404	0.114
C II*	1335.71	4842.79	2.625635	0.000010	4.07	1.56	12.589	0.072
H I	1215.67	4845.44	2.985813	0.000029	63.31	5.08	13.212	0.041
H I	1215.67	4845.49	2.985853	0.000003	21.08	0.50	13.767	0.013
N V	1238.82	4845.63	2.911485	0.000009	1.84	2.06	12.758	0.116
H I	1215.67	4848.44	2.988283	0.000002	22.08	0.31	14.177	0.015
H I	1215.67	4849.28	2.988975	0.000006	5.07	0.94	12.387	0.054
H I	1215.67	4849.82	2.989419	0.000014	23.63	1.69	12.937	0.024
H I	1215.67	4851.69	2.990960	0.000022	33.30	1.15	13.947	0.026
H I	1215.67	4852.16	2.991345	0.000010	12.56	1.47	13.328	0.088
H I	1215.67	4852.93	2.991980	0.000006	21.66	0.56	13.539	0.011
H I	1215.67	4855.40	2.994009	0.000007	26.66	0.49	14.690	0.029
Si IV	1393.76	4855.57	2.483805	0.000003	8.32	0.51	12.875	0.032
Si IV	1393.76	4856.19	2.484248	0.000032	22.30	1.53	13.027	0.084
H I	1215.67	4857.48	2.995722	0.000020	12.89	2.86	12.512	0.128
H I	1215.67	4858.48	2.996544	0.000008	52.18	0.73	14.144	0.006
Si IV	1393.76	4858.68	2.486037	0.000015	35.25	1.84	12.847	0.020
H I	1215.67	4860.72	2.998382	0.000007	33.98	0.81	13.723	0.009
N V	1242.80	4861.21	2.911485	0.000009	1.84	2.06	12.758	0.116
H I	1215.67	4861.53	2.999053	0.000016	14.14	1.82	13.094	0.075
H I	1215.67	4862.27	2.999657	0.000006	23.74	0.77	14.333	0.021
H I	1215.67	4863.23	3.000453	0.000023	18.39	2.23	12.692	0.051
H I	1215.67	4864.71	3.001668	0.000012	21.57	2.09	13.080	0.112
H I	1215.67	4865.28	3.002140	0.000271	40.55	15.24	12.708	0.276

Table 4. Absorption line parameter list

ID	λ_{rest}	λ_{obs}	z	σ_z	b	σ_b	$\text{Log}N$	$\sigma_{\text{Log}N}$
H I	1215.67	4868.81	3.005042	0.000094	93.08	13.04	12.824	0.053
H I	1215.67	4870.75	3.006637	0.000064	32.89	3.43	14.099	0.334
H I	1215.67	4871.32	3.007104	0.000568	43.09	24.65	13.782	0.704
H I	1215.67	4873.02	3.008506	0.000011	19.09	1.88	12.934	0.091
H I	1215.67	4873.32	3.008747	0.000148	67.53	10.46	13.387	0.102
H I	1215.67	4875.33	3.010406	0.000018	40.71	2.35	13.174	0.040
H I	1215.67	4877.55	3.012226	0.000110	95.26	23.85	13.074	0.096
H I	1215.67	4878.97	3.013396	0.000023	27.56	4.23	12.590	0.128
H I	1215.67	4880.95	3.015023	0.000122	57.37	9.68	13.141	0.100
H I	1215.67	4881.77	3.015699	0.000010	27.48	2.23	13.077	0.094
H I	1215.67	4883.41	3.017048	0.000018	46.82	1.85	13.058	0.015
H I	1215.67	4886.56	3.019643	0.000031	41.71	2.39	13.135	0.029
Si IV	1402.77	4886.98	2.483805	0.000003	8.32	0.51	12.875	0.032
Si IV	1402.77	4887.60	2.484248	0.000032	22.30	1.53	13.027	0.084
H I	1215.67	4887.74	3.020615	0.000048	30.33	2.86	13.086	0.065
Si IV	1402.77	4890.11	2.486037	0.000015	35.25	1.84	12.847	0.020
H I	1215.67	4900.63	3.031214	0.000084	60.71	8.43	12.700	0.054
H I	1215.67	4901.87	3.032231	0.000004	24.41	0.48	13.507	0.010
H I	1215.67	4902.70	3.032916	0.000016	24.50	1.46	12.866	0.026
Al II	1670.79	4904.03	1.935159	0.000002	1.73	0.49	11.544	0.024
Al II	1670.79	4904.15	1.935231	0.000004	17.69	0.74	11.895	0.020
Al II	1670.79	4904.17	1.935243	0.000004	1.42	1.50	11.152	0.057
H I	1215.67	4906.97	3.036431	0.000028	15.91	3.63	11.962	0.078
H I	1215.67	4913.35	3.041680	0.000278	70.16	14.94	12.879	0.162
H I	1215.67	4914.29	3.042455	0.000010	35.34	2.29	13.183	0.075
H I	1215.67	4916.42	3.044202	0.000046	42.81	5.01	12.444	0.044
H I	1215.67	4919.75	3.046940	0.000027	16.98	1.50	13.034	0.105
H I	1215.67	4920.17	3.047284	0.000032	19.38	2.20	13.112	0.092
H I	1215.67	4920.37	3.047453	0.000150	45.14	7.73	12.627	0.169
H I	1215.67	4922.82	3.049466	0.000014	10.05	2.02	12.298	0.113
H I	1215.67	4923.11	3.049704	0.000003	29.99	0.20	13.710	0.005
H I	1215.67	4924.95	3.051217	0.000007	9.72	0.86	12.233	0.028
Si II	1260.42	4927.80	2.909643	0.000003	8.10	0.50	12.476	0.035
Si II	1260.42	4928.45	2.910154	0.000011	31.31	1.33	13.266	0.016
Si II	1260.42	4928.46	2.910164	0.000003	7.79	0.22	14.011	0.034
Si II	1260.42	4928.62	2.910289	0.000028	11.42	0.88	13.331	0.132
Si II	1260.42	4929.25	2.910793	0.000002	6.02	0.30	12.414	0.018
Si II	1260.42	4929.65	2.911111	0.000001	10.40	0.19	12.853	0.006
Si II	1260.37	4929.83	2.911411	0.000011	3.70	1.87	11.272	0.095
Ni II	1370.13	4966.87	2.625111	0.000296	31.35	10.65	13.310	0.527
Ni II	1370.13	4967.11	2.625286	0.000016	17.20	3.17	13.532	0.275
Ni II	1370.13	4967.60	2.625646	0.000003	5.33	0.62	13.168	0.063
Ni II	1370.13	4967.88	2.625847	0.000046	15.20	4.54	12.921	0.159
???	5044.30	5044.30	0.000000	0.000007	18.62	3.00	12.358	0.057
Si IV	1393.76	5047.62	2.621594	0.000001	3.46	0.16	12.963	0.016
Si IV	1393.76	5050.93	2.623971	0.000038	34.14	10.45	12.163	0.120
Si IV	1393.76	5051.38	2.624292	0.000003	5.04	0.54	12.811	0.050
Si IV	1393.76	5051.67	2.624499	0.000007	16.75	0.84	13.302	0.021
Si IV	1393.76	5052.60	2.625173	0.000002	20.04	0.30	14.026	0.007
Si IV	1393.76	5053.21	2.625607	0.000005	6.22	0.83	12.607	0.055
Si IV	1393.76	5053.70	2.625958	0.000011	29.66	1.20	13.247	0.016
Si IV	1402.77	5080.27	2.621594	0.000001	3.46	0.16	12.963	0.016
Si IV	1402.77	5083.60	2.623971	0.000038	34.14	10.45	12.163	0.120
Si IV	1402.77	5084.05	2.624292	0.000003	5.04	0.54	12.811	0.050
Si IV	1402.77	5084.34	2.624499	0.000007	16.75	0.84	13.302	0.021
Si IV	1402.77	5085.29	2.625173	0.000002	20.04	0.30	14.026	0.007
Si IV	1402.77	5085.89	2.625607	0.000005	6.22	0.83	12.607	0.055
Si IV	1402.77	5086.39	2.625958	0.000011	29.66	1.20	13.247	0.016
O I	1302.17	5091.02	2.909643	0.000000	10.73	0.00	13.000	0.062
O I	1302.17	5091.69	2.910164	0.000000	10.33	0.00	14.837	0.043
O I	1302.17	5091.86	2.910289	0.000000	15.14	0.00	14.229	0.116
O I	1302.17	5092.51	2.910793	0.000000	7.97	0.00	12.460	0.187
O I	1302.17	5092.93	2.911111	0.000000	13.78	0.00	13.002	0.067

Table 4. Absorption line parameter list

ID	λ_{rest}	λ_{obs}	z	σ_z	b	σ_b	$\text{Log}N$	$\sigma_{\text{Log}N}$
Si II	1304.37	5099.62	2.909643	0.000003	8.10	0.50	12.476	0.035
Si II	1304.37	5100.29	2.910154	0.000011	31.31	1.33	13.266	0.016
Si II	1304.37	5100.30	2.910164	0.000003	7.79	0.22	14.011	0.034
Si II	1304.37	5100.47	2.910289	0.000028	11.42	0.88	13.331	0.132
Si II	1304.37	5101.12	2.910793	0.000002	6.02	0.30	12.414	0.018
Si II	1304.37	5101.54	2.911111	0.000001	10.40	0.19	12.853	0.006
Si II	1304.37	5101.92	2.911411	0.000011	3.70	1.87	11.272	0.095
C II	1334.53	5134.40	2.847341	0.000007	6.02	0.87	12.808	0.039
C II	1334.53	5137.44	2.849618	0.000004	4.55	0.70	13.191	0.051
C II	1334.53	5137.48	2.849649	0.000007	21.80	1.12	13.609	0.020
C II	1334.53	5138.33	2.850285	0.000025	10.04	3.26	12.477	0.105
C II	1334.53	5217.56	2.909653	0.000014	8.96	4.01	13.283	0.433
C II	1334.53	5218.17	2.910111	0.000290	25.80	26.69	13.833	0.810
C II	1334.53	5218.30	2.910207	0.000013	14.47	2.49	14.444	0.223
C II	1334.53	5219.10	2.910809	0.000005	8.04	0.80	13.378	0.042
C II	1334.53	5219.51	2.911114	0.000003	9.82	0.55	13.755	0.015
C II	1334.53	5219.87	2.911388	0.000023	6.18	2.94	12.496	0.148
Ni II	1454.84	5273.96	2.625111	0.000296	31.35	10.65	13.310	0.527
Ni II	1454.84	5274.21	2.625286	0.000016	17.20	3.17	13.532	0.275
Ni II	1454.84	5274.73	2.625646	0.000003	5.33	0.62	13.168	0.063
Ni II	1454.84	5275.03	2.625847	0.000046	15.20	4.54	12.921	0.159
Si II	1526.71	5318.52	2.483654	0.000009	13.65	0.94	13.072	0.029
Si II	1526.71	5318.84	2.483862	0.000007	4.78	1.35	12.479	0.096
Si II	1526.71	5319.16	2.484076	0.000003	6.96	0.40	13.032	0.016
C IV	1548.20	5324.27	2.439015	0.000004	11.07	0.49	12.870	0.015
C IV	1550.77	5333.12	2.439015	0.000004	11.07	0.49	12.870	0.015
Si IV	1393.76	5344.46	2.834577	0.000010	16.74	1.15	12.481	0.024
Si IV	1393.76	5360.29	2.845935	0.000009	9.23	1.25	12.242	0.054
Si IV	1393.76	5360.92	2.846389	0.000016	14.54	2.13	12.254	0.057
Si IV	1393.76	5361.60	2.846877	0.000029	9.93	3.74	11.764	0.140
Si IV	1393.76	5362.27	2.847356	0.000002	6.16	0.19	12.934	0.011
Si IV	1393.76	5362.92	2.847818	0.000009	13.74	1.12	12.511	0.032
Si IV	1393.76	5365.16	2.849430	0.000004	1.58	0.47	12.693	0.062
Si IV	1393.76	5365.22	2.849471	0.000013	32.75	0.85	13.357	0.020
Si IV	1393.76	5365.41	2.849608	0.000002	7.22	0.32	13.585	0.013
Si IV	1393.76	5365.77	2.849866	0.000003	6.48	0.38	12.997	0.023
Si IV	1402.77	5379.03	2.834577	0.000010	16.74	1.15	12.481	0.024
C IV	1548.19	5389.02	2.480842	0.000028	26.85	3.63	12.771	0.056
C IV	1548.19	5393.59	2.483793	0.000005	9.33	0.94	12.815	0.051
C IV	1548.19	5394.11	2.484130	0.000002	6.82	0.33	13.139	0.021
C IV	1548.19	5394.21	2.484194	0.000025	43.94	2.07	13.360	0.028
Si IV	1402.77	5394.96	2.845935	0.000009	9.23	1.25	12.242	0.054
Si IV	1402.77	5395.60	2.846389	0.000016	14.54	2.13	12.254	0.057
Si IV	1402.77	5396.28	2.846877	0.000029	9.93	3.74	11.764	0.140
C IV	1548.20	5396.62	2.485746	0.000026	12.54	3.64	12.224	0.103
Si IV	1402.77	5396.95	2.847356	0.000002	6.16	0.19	12.934	0.011
Si IV	1402.77	5397.60	2.847818	0.000009	13.74	1.12	12.511	0.032
C IV	1548.20	5397.61	2.486386	0.000006	20.01	0.62	13.379	0.013
C IV	1548.20	5397.94	2.486600	0.000004	2.41	1.00	12.415	0.061
C IV	1550.77	5397.99	2.480842	0.000028	26.85	3.63	12.771	0.056
Si IV	1402.77	5399.87	2.849430	0.000004	1.58	0.47	12.693	0.062
Si IV	1402.77	5399.92	2.849471	0.000013	32.75	0.85	13.357	0.020
Si IV	1402.77	5400.11	2.849608	0.000002	7.22	0.32	13.585	0.013
Si IV	1402.77	5400.48	2.849866	0.000003	6.48	0.38	12.997	0.023
C IV	1550.77	5402.56	2.483793	0.000005	9.33	0.94	12.815	0.051
C IV	1550.77	5403.09	2.484130	0.000002	6.82	0.33	13.139	0.021
C IV	1550.77	5403.18	2.484194	0.000025	43.94	2.07	13.360	0.028
C IV	1550.77	5405.59	2.485746	0.000026	12.54	3.64	12.224	0.103
C IV	1550.77	5406.58	2.486386	0.000006	20.01	0.62	13.379	0.013
C IV	1550.77	5406.92	2.486600	0.000004	2.41	1.00	12.415	0.061
Al III	1854.72	5443.90	1.935163	0.000003	5.93	0.45	12.219	0.020
Si IV	1393.76	5449.90	2.910228	0.000007	27.87	0.85	12.990	0.011
Si IV	1393.76	5450.74	2.910827	0.000003	7.62	0.38	12.731	0.021

Table 4. Absorption line parameter list

ID	λ_{rest}	λ_{obs}	z	σ_z	b	σ_b	Log N	$\sigma_{\text{Log}N}$
Si IV	1393.76	5451.29	2.911224	0.000006	21.18	0.71	13.073	0.011
Si IV	1393.76	5452.68	2.912224	0.000023	14.36	2.82	12.051	0.065
Si IV	1393.76	5453.42	2.912751	0.000011	13.01	1.38	12.306	0.035
Al III	1862.79	5467.59	1.935163	0.000003	5.93	0.45	12.219	0.020
Si IV	1402.77	5485.15	2.910228	0.000007	27.87	0.85	12.990	0.011
Si IV	1402.77	5485.99	2.910827	0.000003	7.62	0.38	12.731	0.021
Si IV	1402.77	5486.55	2.911224	0.000006	21.18	0.71	13.073	0.011
Si IV	1402.77	5487.95	2.912224	0.000023	14.36	2.82	12.051	0.065
Si IV	1402.77	5488.69	2.912751	0.000011	13.01	1.38	12.306	0.035
Fe II	2344.21	5504.06	1.347933	0.000002	3.97	0.48	12.108	0.023
Fe II	2344.21	5504.50	1.348120	0.000001	4.55	0.28	12.386	0.014
Fe II	2344.21	5505.46	1.348531	0.000001	6.55	0.11	12.996	0.006
Si II	1526.71	5533.34	2.624365	0.000003	10.63	0.28	13.410	0.012
Si II	1526.71	5533.73	2.624617	0.000003	3.27	0.33	13.076	0.025
Si II	1526.71	5534.73	2.625274	0.000007	16.77	0.28	16.655	0.040
Si II	1526.71	5535.66	2.625883	0.000009	9.60	0.57	14.167	0.040
Si II	1526.71	5536.16	2.626211	0.000009	8.58	1.01	12.602	0.046
Fe II	2374.46	5575.08	1.347933	0.000002	3.97	0.48	12.108	0.023
Fe II	2374.46	5575.52	1.348120	0.000001	4.55	0.28	12.386	0.014
Fe II	2374.46	5576.50	1.348531	0.000001	6.55	0.11	12.996	0.006
Fe II	2382.77	5594.57	1.347933	0.000002	3.97	0.48	12.108	0.023
Fe II	2382.77	5595.02	1.348120	0.000001	4.55	0.28	12.386	0.014
Fe II	2382.77	5596.00	1.348531	0.000001	6.55	0.11	12.996	0.006
Fe II	1608.45	5603.05	2.483501	0.000027	12.05	3.56	12.700	0.099
C IV	1548.20	5606.90	2.621572	0.000001	7.57	0.13	13.593	0.007
C IV	1548.20	5610.58	2.623949	0.000020	9.12	3.50	12.216	0.176
C IV	1548.20	5611.15	2.624319	0.000003	4.82	0.36	13.233	0.025
C IV	1548.20	5611.49	2.624535	0.000002	7.56	0.25	14.002	0.016
C IV	1548.20	5612.44	2.625150	0.000003	18.90	0.47	14.193	0.014
C IV	1548.20	5612.54	2.625216	0.000018	72.34	1.73	14.146	0.022
C IV	1548.20	5613.16	2.625618	0.000008	5.54	1.58	12.604	0.108
C IV	1548.20	5613.68	2.625953	0.000007	6.19	1.27	12.616	0.074
C IV	1550.77	5616.23	2.621572	0.000001	7.57	0.13	13.593	0.007
C IV	1550.77	5619.91	2.623949	0.000020	9.12	3.50	12.216	0.176
C IV	1550.77	5620.49	2.624319	0.000003	4.82	0.36	13.233	0.025
C IV	1550.77	5620.82	2.624535	0.000002	7.56	0.25	14.002	0.016
C IV	1550.77	5621.77	2.625150	0.000003	18.90	0.47	14.193	0.014
C IV	1550.77	5621.88	2.625216	0.000018	72.34	1.73	14.146	0.022
C IV	1550.77	5622.50	2.625618	0.000008	5.54	1.58	12.604	0.108
C IV	1550.77	5623.02	2.625953	0.000007	6.19	1.27	12.616	0.074
???	5675.65	5675.65	0.000000	0.000003	18.49	1.19	12.539	0.023
???	5677.58	5677.58	0.000000	0.000002	12.63	0.84	12.514	0.023
Al II	1670.79	5820.61	2.483754	0.000006	17.88	0.83	12.161	0.016
Al II	1670.79	5821.19	2.484100	0.000004	8.44	0.61	11.844	0.027
Fe II	1608.45	5829.66	2.624384	0.000023	15.00	3.39	12.760	0.077
Fe II	1608.45	5830.95	2.625190	0.000003	22.47	0.29	14.785	0.008
Fe II	1608.45	5831.69	2.625649	0.000005	6.31	1.02	14.284	0.122
Fe II	1608.45	5831.90	2.625782	0.000177	12.73	7.26	13.637	0.492
Fe II	1608.45	5832.15	2.625936	0.000005	3.26	1.28	13.256	0.156
Fe II	1611.20	5839.61	2.624384	0.000023	15.00	3.39	12.760	0.077
Fe II	1611.20	5840.91	2.625190	0.000003	22.47	0.29	14.785	0.008
Fe II	1611.20	5841.65	2.625649	0.000005	6.31	1.02	14.284	0.122
Fe II	1611.20	5841.86	2.625782	0.000177	12.73	7.26	13.637	0.492
Fe II	1611.20	5842.11	2.625936	0.000005	3.26	1.28	13.256	0.156
C IV	1548.20	5863.24	2.787147	0.000010	10.11	1.21	12.457	0.038
C IV	1550.77	5872.99	2.787147	0.000010	10.11	1.21	12.457	0.038
C IV	1548.20	5875.57	2.795109	0.000012	15.73	1.38	12.779	0.031
C IV	1548.20	5877.02	2.796049	0.000046	29.07	5.47	12.554	0.067
C IV	1550.77	5885.34	2.795109	0.000012	15.73	1.38	12.779	0.031
C IV	1550.77	5886.80	2.796049	0.000046	29.07	5.47	12.554	0.067
Na I	5891.58	5890.67	-0.000154	0.000000	4.18	0.22	11.920	0.012
Na I	5891.58	5891.07	-0.000087	0.000001	1.78	0.17	12.121	0.046
Na I	5891.58	5891.27	-0.000052	0.000001	3.16	0.34	12.044	0.015

Table 4. Absorption line parameter list

ID	λ_{rest}	λ_{obs}	z	σ_z	b	σ_b	$\text{Log}N$	$\sigma_{\text{Log}N}$
Na I	5897.56	5896.65	-0.000154	0.000000	4.18	0.22	11.920	0.012
Na I	5897.56	5897.04	-0.000087	0.000001	1.78	0.17	12.121	0.046
Na I	5897.56	5897.25	-0.000052	0.000001	3.16	0.34	12.044	0.015
C IV	1548.20	5935.78	2.834001	0.000010	6.26	1.37	12.135	0.058
C IV	1548.20	5936.57	2.834510	0.000008	12.45	0.65	13.242	0.027
C IV	1548.20	5936.92	2.834737	0.000009	8.38	0.82	12.854	0.063
C IV	1548.20	5937.45	2.835077	0.000009	4.22	1.45	12.005	0.070
C IV	1548.20	5938.24	2.835591	0.000018	18.52	2.07	12.517	0.039
C IV	1550.77	5945.65	2.834001	0.000010	6.26	1.37	12.135	0.058
C IV	1550.77	5946.44	2.834510	0.000008	12.45	0.65	13.242	0.027
C IV	1550.77	5946.79	2.834737	0.000009	8.38	0.82	12.854	0.063
C IV	1550.77	5947.32	2.835077	0.000009	4.22	1.45	12.005	0.070
C IV	1550.77	5948.12	2.835591	0.000018	18.52	2.07	12.517	0.039
C IV	1548.20	5954.25	2.845932	0.000006	12.33	0.83	12.846	0.031
C IV	1548.20	5955.16	2.846521	0.000007	4.42	1.18	12.364	0.072
C IV	1548.20	5955.52	2.846752	0.000020	40.98	2.52	13.502	0.021
C IV	1548.20	5956.47	2.847366	0.000002	13.21	0.29	13.690	0.011
C IV	1548.20	5957.22	2.847850	0.000001	13.48	0.19	14.002	0.005
C IV	1548.20	5957.83	2.848243	0.000004	9.22	0.65	13.102	0.028
C IV	1548.20	5958.44	2.848638	0.000060	15.44	7.92	12.667	0.220
C IV	1548.20	5958.75	2.848837	0.000003	5.07	0.59	13.111	0.058
C IV	1548.20	5959.76	2.849493	0.000004	27.96	0.47	14.869	0.024
C IV	1548.20	5960.43	2.849925	0.000011	5.17	1.09	13.430	0.089
C IV	1548.20	5961.17	2.850403	0.000029	13.89	3.51	12.403	0.093
C IV	1550.77	5964.15	2.845932	0.000006	12.33	0.83	12.846	0.031
C IV	1550.77	5965.07	2.846521	0.000007	4.42	1.18	12.364	0.072
C IV	1550.77	5965.43	2.846752	0.000020	40.98	2.52	13.502	0.021
C IV	1550.77	5966.38	2.847366	0.000002	13.21	0.29	13.690	0.011
C IV	1550.77	5967.13	2.847850	0.000001	13.48	0.19	14.002	0.005
C IV	1550.77	5967.74	2.848243	0.000004	9.22	0.65	13.102	0.028
C IV	1550.77	5968.35	2.848638	0.000060	15.44	7.92	12.667	0.220
C IV	1550.77	5968.66	2.848837	0.000003	5.07	0.59	13.111	0.058
Si II	1526.71	5968.88	2.909643	0.000003	8.10	0.50	12.476	0.035
Si II	1526.71	5969.66	2.910154	0.000011	31.31	1.33	13.266	0.016
Si II	1526.71	5969.67	2.910164	0.000003	7.79	0.22	14.011	0.034
C IV	1550.77	5969.68	2.849493	0.000004	27.96	0.47	14.869	0.024
Si II	1526.71	5969.86	2.910289	0.000028	11.42	0.88	13.331	0.132
C IV	1550.77	5970.35	2.849925	0.000011	5.17	1.09	13.430	0.089
Si II	1526.71	5970.63	2.910793	0.000002	6.02	0.30	12.414	0.018
C IV	1550.77	5971.09	2.850403	0.000029	13.89	3.51	12.403	0.093
Si II	1526.71	5971.12	2.911111	0.000001	10.40	0.19	12.853	0.006
Si II	1526.71	5971.58	2.911411	0.000011	3.70	1.87	11.272	0.095
C IV	1548.20	6030.89	2.895431	0.000005	5.05	0.63	12.482	0.048
C IV	1548.20	6031.23	2.895651	0.000004	10.53	0.41	13.115	0.013
C IV	1548.20	6033.84	2.897340	0.000009	17.50	1.03	12.734	0.021
C IV	1550.77	6040.92	2.895431	0.000005	5.05	0.63	12.482	0.048
C IV	1550.77	6041.26	2.895651	0.000004	10.53	0.41	13.115	0.013
C IV	1550.77	6043.88	2.897340	0.000009	17.50	1.03	12.734	0.021
Al II	1670.79	6053.75	2.623293	0.000017	17.88	2.32	11.610	0.065
C IV	1548.20	6055.41	2.911272	0.000016	49.83	1.87	13.722	0.018
Al II	1670.79	6055.54	2.624366	0.000004	12.16	0.51	12.433	0.016
C IV	1548.20	6055.62	2.911406	0.000022	16.19	2.89	13.087	0.097
C IV	1548.20	6055.96	2.911626	0.000003	3.81	0.77	12.777	0.070
Al II	1670.79	6057.16	2.625336	0.000010	25.60	0.61	14.207	0.053
Al II	1670.79	6058.19	2.625950	0.000003	3.14	0.74	12.372	0.055
Al II	1670.79	6058.21	2.625965	0.000151	17.13	6.83	12.115	0.479
C IV	1548.20	6060.85	2.914786	0.000011	10.76	1.29	12.595	0.043
C IV	1548.20	6061.37	2.915124	0.000003	10.54	0.42	13.283	0.015
C IV	1548.20	6061.99	2.915521	0.000014	16.99	1.71	12.832	0.035
C IV	1548.20	6063.19	2.916300	0.000007	16.83	0.81	12.916	0.017
C IV	1550.77	6065.48	2.911272	0.000016	49.83	1.87	13.722	0.018
C IV	1550.77	6065.69	2.911406	0.000022	16.19	2.89	13.087	0.097
C IV	1550.77	6066.03	2.911626	0.000003	3.81	0.77	12.777	0.070

Table 4. Absorption line parameter list

ID	λ_{rest}	λ_{obs}	z	σ_z	b	σ_b	$\text{Log}N$	$\sigma_{\text{Log}N}$
C IV	1550.77	6070.93	2.914786	0.000011	10.76	1.29	12.595	0.043
C IV	1550.77	6071.46	2.915124	0.000003	10.54	0.42	13.283	0.015
C IV	1550.77	6072.07	2.915521	0.000014	16.99	1.71	12.832	0.035
C IV	1550.77	6073.24	2.916300	0.000007	16.83	0.81	12.916	0.017
Fe II	2586.65	6073.28	1.347933	0.000002	3.97	0.48	12.108	0.023
Fe II	2586.65	6073.76	1.348120	0.000001	4.55	0.28	12.386	0.014
Fe II	2586.65	6074.83	1.348531	0.000001	6.55	0.11	12.996	0.006
Fe II	2600.17	6105.03	1.347933	0.000002	3.97	0.48	12.108	0.023
Fe II	2600.17	6105.52	1.348120	0.000001	4.55	0.28	12.386	0.014
Fe II	2600.17	6106.59	1.348531	0.000001	6.55	0.11	12.996	0.006
Ni II	1709.60	6197.49	2.625111	0.000296	31.35	10.65	13.310	0.527
Ni II	1709.60	6197.79	2.625286	0.000016	17.20	3.17	13.532	0.275
Ni II	1709.60	6198.40	2.625646	0.000003	5.33	0.62	13.168	0.063
Ni II	1709.60	6198.75	2.625847	0.000046	15.20	4.54	12.921	0.159
Fe II	1608.45	6289.37	2.910193	0.000003	10.10	0.28	13.658	0.010
Ni II	1741.55	6313.31	2.625111	0.000296	31.35	10.65	13.310	0.527
Ni II	1741.55	6313.62	2.625286	0.000016	17.20	3.17	13.532	0.275
Ni II	1741.55	6314.24	2.625646	0.000003	5.33	0.62	13.168	0.063
Ni II	1741.55	6314.59	2.625847	0.000046	15.20	4.54	12.921	0.159
Ni II	1751.91	6350.87	2.625111	0.000296	31.35	10.65	13.310	0.527
Ni II	1751.91	6351.17	2.625286	0.000016	17.20	3.17	13.532	0.275
Ni II	1751.91	6351.81	2.625646	0.000003	5.33	0.62	13.168	0.063
Ni II	1751.91	6352.16	2.625847	0.000046	15.20	4.54	12.921	0.159
Al II	1670.79	6532.37	2.909758	0.000013	14.67	1.71	11.773	0.038
Al II	1670.79	6533.10	2.910197	0.000002	9.85	0.25	12.762	0.009
Al II	1670.79	6533.58	2.910481	0.000007	4.52	0.98	11.519	0.050
Al II	1670.79	6534.16	2.910826	0.000004	3.23	0.60	11.612	0.031
Al II	1670.79	6534.62	2.911105	0.000007	10.30	0.95	11.862	0.028